FERONIA promotes PUB25/PUB26-mediated ubiquitination of ATG1 to restrain nitrogen starvation-induced autophagy

Qiuling Wang

wangqiuling@nwafu.edu.cn

Northwest A&F University https://orcid.org/0000-0002-1066-5909

Shujuan Guo

Northwest A&F University

Yushi Peng

Northwest A&F University

Tongyao Yang

Northwest A&F University

Na Li

Lanzhou University

Tong Liu

Northwest A&F University

Suiwen Hou

Lanzhou University

Linhui Yu

Northwest A&F University

Article

Keywords: autophagy, PUB25, PUB26, FERONIA, ATG1, ATG13, nitrogen starvation, ubiquitination, phosphorylation

Posted Date: May 19th, 2026

DOI: https://doi.org/10.21203/rs.3.rs-9554211/v1

Additional Declarations: There is **NO** Competing Interest.

RESEARCH ARTICLE

FERONIA promotes PUB25/PUB26-mediated ubiquitination of ATG1 to restrain nitrogen starvation-induced autophagy

Qiuling Wang[1,†,*], Shujuan Guo[1,†], Yushi Peng[1], Tongyao Yang[1], Na Li[2], Tong Liu[1] Suiwen Hou[2,*], Linhui Yu[1,*]

[1] Institute of Future Agriculture, State Key Laboratory of Crop Stress Biology for Arid Areas, Northwest A&F University, Yangling 712100, Shaanxi, People's Republic of China

[2] Key Laboratory of Cell Activities and Stress Adaptations, Ministry of Education, School of Life Sciences, Lanzhou University, Lanzhou 730000, People's Republic of China

† These authors contributed equally.

*Author for correspondence: Qiuling Wang (wangqiuling@nwafu.edu.cn), Suiwen Hou (housw@lzu.edu.cn), Linhui Yu (yulh@nwafu.edu.cn)

Abstract

Autophagy must be dynamically tuned to nutrient availability, yet how plants prevent excessive autophagy during nutrient starvation while preserving basal flux under replete conditions remains elusive. Here, we identify the redundant U-box E3 ligases PUB25 and PUB26 as critical negative regulators of nitrogen starvation-induced autophagy in Arabidopsis. Loss of PUB25/PUB26 enhances autophagy and improves plant growth under nitrogen deprivation, whereas their overexpression suppresses autophagy. Mechanistically, PUB25/PUB26 directly interacts with the autophagy-initiating kinase ATG1 and target it for proteasomal degradation. During nitrogen starvation, the receptor kinase FERONIA (FER) is transcriptionally upregulated and enhances PUB25/PUB26 activity by phosphorylating it at Thr95/Thr94, acting as a

molecular brake on ATG1 to fine-tune autophagy to proper cellular levels during prolonged deprivation. Additionally, under nitrogen-rich conditions, FER directly phosphorylates ATG13 to repress ATG1-ATG13 complex assembly, thereby sustaining low basal autophagy. Together, our findings reveal a nutrient-responsive FER-PUB25/PUB26 regulatory module that integrates constitutive and inducible regulatory checkpoints to dynamically modulate autophagy activity across variable nitrogen status, optimizing plant fitness.

Key words: autophagy; PUB25; PUB26; FERONIA; ATG1; ATG13; nitrogen starvation; ubiquitination; phosphorylation

Introduction

Autophagy is a highly conserved degradation and recycling pathway that removes damaged proteins and organelles to maintain cellular homeostasis, playing critical roles in plant stress adaptation, growth, development, and immune regulation[1]. The execution of autophagy relies on the coordinated action of autophagy-related (ATG) proteins, which assemble into functional complexes to drive autophagosome formation[2,3]. Autophagy initiation depends on the ATG1-ATG13 kinase complex, which functions as the master regulatory switch for autophagy induction[4,5]. In *Arabidopsis thaliana,* this complex consists of the serine/threonine kinase ATG1 and its regulatory subunits ATG13, ATG11, and ATG101[6,7]. Loss-of-function mutations in these components restrict autophagy and enhance sensitivity to nutrient deficiency, leading to premature leaf senescence and shortened lifespan, highlighting their essential roles in stress adaptation[6-9].

The activity of the ATG1 complex is primarily regulated by phosphorylation. Under nutrient-sufficient conditions, the activated target of rapamycin (TOR) kinase is generally thought to hyperphosphorylate ATG13, preventing ATG1-ATG13 complex

assembly and inhibiting autophagy[10,11]. When plants encounter nutrient starvation, the plant energy sensor SNF1-related protein kinase (SnRK1) activates autophagy by directly phosphorylating ATG1 and inhibiting TOR activity[11-13]. Our previous research revealed that type one protein phosphatase (TOPP) positively regulates the formation of the ATG1-ATG13 complex by dephosphorylating ATG13 at multiple phosphorylation sites[14].

While phosphorylation enables rapid on-off switching of autophagy, accumulating evidence indicates that the ubiquitin-proteasome system (UPS) provides fine-tuning of autophagy by controlling the stability of this complex[15,16]. In mammalian cells, the unc-51-like autophagy-activating kinase 1 (ULK1) complex is regulated by ubiquitination mediated by various E3 ligases. Short-term starvation promotes K63-linked ubiquitination, stabilizing the complex and activating autophagy[17,18], whereas prolonged starvation triggers K48-linked ubiquitination, leading to proteasomal degradation of ULK1 to terminate autophagy[19-23]. Similar regulatory mechanisms also target other complex components, such as ATG13 and ATG101[24,25]. In plants, ATG1 and ATG13 also undergo proteasomal degradation during prolonged starvation and recovery[6,8,26]. ATG13 degradation is mainly mediated by SINAT1 and SINAT2, which are E3 ubiquitin ligases of the SINAT (seven in absentia of *Arabidopsis thaliana*) family. They ubiquitinate ATG13 to keep autophagy low under nutrient-rich conditions, attenuate hyperactivated autophagy during starvation, and terminate autophagy upon recovery[8]. However, it remains unknown whether other E3 ligases target the ATG1 complex, particularly its core kinase subunit ATG1.

Plant U-box (PUB) E3 ubiquitin ligases represent a large plant-specific protein family involved in various biological processes, including plant growth, development, and stress responses[27-31]. Among these, PUB25 and PUB26 are versatile signaling hubs

with diverse functions. They regulate plant cold adaptation by targeting the transcription factors ICE1 and MYB15[32,33], suppress immune signaling by degrading the receptor-like cytoplasmic kinase BOTRYTIS-INDUCED KINASE 1 (BIK1), transcription factor MYB6, and the RING domain E3 ligase (RGLG1/2) for degradation[34-36], and positively regulate ABA signaling by promoting the degradation of BR signaling kinase 1 (BSK1)[37]. Moreover, they are also implicated in plant development, miRNA processing, salt stress responses, and anthocyanin biosynthesis[38-41]. Notably, the activity of PUB25 and PUB26 is tightly regulated by upstream kinases such as OST1, CPK28, and BAK1[32,34,37]. A recent proteomic screen identified PUB25 and PUB26 as putative interactors of the receptor-like kinase FERONIA (FER)[42], suggesting a potential regulatory link between them.

FER is a member of the Catharanthus roseus receptor-like kinase 1-like (CrRLK1L) family and functions as a key signaling hub regulating diverse biological processes, including plant fertilization, immune responses, and adaptation to abiotic stresses[43-45]. Studies have demonstrated that the *fer-4* mutant exhibits constitutive autophagy even under non-stress conditions[46]. Approximately 36% of autophagy-related genes in *fer-4* show alterations at the transcript or protein level, including TOR, the negative regulator of autophagy[10,47]. FER physically interacts with the TOR kinase complex, and *fer* mutants show reduced TOR activity[48,49]. These findings indicate that FER negatively regulates autophagy at least partially through the TOR pathway, as reduced TOR activity contributes to the constitutive autophagy observed in *fer* mutants[46,47], Yet, whether FER modulates autophagy through TOR-independent mechanisms remains unknown. In the current study, we identify the U-box E3 ligases PUB25 and PUB26 as negative regulators of autophagy that act downstream of FER to target ATG1 for degradation under nitrogen starvation. Furthermore, we demonstrate that FER directly

phosphorylates ATG13 under nitrogen-rich conditions, thereby constitutively suppressing ATG1-ATG13 complex assembly. Our work uncovers a previously uncharacterized regulatory network that enables plants to precisely modulate autophagy activity in response to nitrogen availability.

Results

PUB25 and PUB26 negatively regulate nitrogen starvation-induced autophagy

Autophagy-related mutants often exhibit altered tolerance to nutrient starvation, particularly carbon and nitrogen deficiency[6,8,9]. To identify regulatory components of autophagy, we conducted a genetic screen on a collection of T-DNA insertion mutants for altered responses to nitrogen starvation. This led to the identification of null mutants of PUB25 and PUB26, two closely related U-box E3 ubiquitin ligases (Supplementary Fig. 1a, b). Whereas single mutants of *pub25* and *pub26* were indistinguishable from wild-type plants, the *pub25 pub26* double mutant exhibited enhanced tolerance to nitrogen starvation (Fig. 1a-d). Reintroduction of *PUB25* or *PUB26* driven by their native promoters into *pub25 pub26* rescued this enhanced tolerance (Supplementary Fig. 1c-g), indicating that the two genes act redundantly. Conversely, *PUB25* and *PUB26* overexpression lines were hypersensitive to nitrogen starvation, a phenotype similar to that of the autophagy-deficient *atg1abct* quadruple mutant (Fig. 1a-d and Supplementary Fig. 1h, i). To dissect the genetic relationship between PUB25/PUB26 and the core autophagy pathway, we generated higher-order mutants by crossing *pub25 pub26* with the autophagy-defective mutants *atg5-1* and *atg7-3*. The enhanced nitrogen starvation tolerance conferred by the *pub25 pub26* mutations was largely abolished in both autophagy-deficient backgrounds (Supplementary Fig. 2), suggesting that PUB25 and PUB26 function upstream of the core autophagy machinery.

We next examined whether PUB25 and PUB26 directly regulate autophagy

activity. The autophagy reporter line *proATG8a::GFP-ATG8a* was crossed into *pub25 pub26* and *PUB25/PUB26* overexpression backgrounds. Confocal microscopy showed that under nitrogen starvation, GFP-ATG8a-labeled puncta were more abundant in root cells of *pub25 pub26* and reduced in *PUB25/PUB26* overexpression lines compared with the wild type (Fig. 1e, f). Consistently, autophagy activity, monitored by free GFP release from GFP-ATG8a[50,51], was enhanced in *pub25 pub26* and reduced in *PUB25* and *PUB26* overexpression lines (Fig. 1g, h). Immunoblot analysis further showed that *pub25 pub26* accumulated higher levels of both lipidated (ATG8a-PE) and non-lipidated ATG8a under nitrogen starvation, whereas *PUB25/PUB26* overexpression suppressed ATG8a accumulation (Fig. 1i, j). Together, these data demonstrate that PUB25 and PUB26 negatively regulate autophagy under nitrogen starvation.

Given this inhibitory function, we investigated whether PUB25 and PUB26 similarly regulate autophagy under carbon-starvation conditions. Unexpectedly, the *pub25 pub26* double mutant exhibited hypersensitivity to both fixed-carbon starvation and dark-induced starvation, while *PUB25* and *PUB26* overexpression conferred increased stress tolerance (Supplementary Fig. 3). Consistent with these phenotypes, autophagy activity was slightly reduced in *pub25 pub26* and moderately increased in *PUB25* and *PUB26* overexpression lines under fixed-carbon starvation (Supplementary Fig. 4). These observations indicate that PUB25 and PUB26 play distinct roles in the regulation of autophagy induced by carbon and nitrogen starvation.

PUB25 and PUB26 associate with autophagosomes via direct interaction with ATG1 kinase

To investigate the mechanism by which PUB25 and PUB26 regulate autophagy, we first tested whether they act at the transcriptional level, given their established role in miRNA processing[39]. qRT-PCR analysis showed comparable transcript levels of *ATGs*

in Col-0 and *pub25 pub26* under nitrogen starvation (Supplementary Fig. 5), indicating that PUB25 and PUB26 do not modulate autophagy through transcriptional regulation.

As PUB25 and PUB26 function as U-box E3 ubiquitin ligases, we performed a yeast two-hybrid (Y2H) screen using a C-terminal fragment of PUB26 ($PUB26^{80–421}$) lacking the U-box domain as bait (Fig. 2a). ATG1a, a core component of the ATG1-ATG13 complex, was identified as a candidate interactor. Y2H and pull-down assays confirmed that PUB25 and PUB26 physically interact with ATG1a in vitro through their C-terminal domains, independent of the U-box (Fig. 2b, c). Co-immunoprecipitation (Co-IP) assays further verified this interaction in planta (Fig. 2d). Additional Y2H, split-luciferase (split-LUC) and bimolecular fluorescence complementation (BiFC) assays showed that PUB25/PUB26 also associates with ATG1b and ATG1c, but not with the truncated isoform ATG1t (Fig. 2e, f and Supplementary Fig. 6a).

To further validate these findings, we performed immunoprecipitation-mass spectrometry (IP-MS) using *pub25 pub26* plants stably expressing proPUB26::PUB26-MYC. ATG1a was co-immunoprecipitated with PUB26-MYC (Supplementary Fig. 6b and Supplementary Data 1), consistent with our previous protein interaction assays. Notably, additional ATG proteins, including ATG18h, ATG13a, ATG4a, ATG11, and ATG6, were also co-immunoprecipitated with PUB26 (Supplementary Fig. 6b and Supplementary Data 1). Follow-up Y2H assays showed that PUB25 interacts with ATG6 and ATG18h, whereas PUB26 binds ATG6, ATG13a, ATG13b, and ATG18h (Supplementary Fig. 6c). Given the complex formation between ATG1 and ATG13, BiFC and split-LUC assays further verified that PUB25/PUB26 associates with ATG13a and ATG13b in vivo (Supplementary Fig. 6d, e). Collectively, these results suggest that PUB25 and PUB26 may regulate autophagy by targeting the ATG1-ATG13 complex.

The interaction of PUB25/PUB26 with ATG proteins prompted us to examine their subcellular localization. Confocal microscopy of PUB25-GFP and PUB26-GFP expressed in Arabidopsis protoplasts revealed predominant cytoplasmic and nuclear localization, together with punctate signals of varying sizes (Supplementary Fig. 7). Co-expression of PUB25/PUB26-GFP with the autophagosome marker RFP-ATG8a revealed strong co-localization (Fig. 2g), demonstrating that PUB25 and PUB26 associate with autophagosomes in vivo.

PUB25 and PUB26 ubiquitinate ATG1 for proteasomal degradation to restrain nitrogen starvation-induced autophagy

Given that PUB25 and PUB26 are E3 ubiquitin ligases that interact with ATG1, we tested whether they directly ubiquitinate ATG1. In vitro ubiquitination assays showed that both PUB25 and PUB26 undergo autoubiquitination and catalyze the ubiquitination of ATG1a (Fig. 3a). Co-expression of PUB25/PUB26 with ATG1a in Arabidopsis protoplasts resulted in ATG1a ubiquitination in vivo (Fig. 3b). To examine ATG1a ubiquitination under physiological conditions, we introduced proATG1a::YFP-ATG1a into *pub25 pub26* and *PUB25/PUB26* overexpression lines. Under nitrogen starvation, polyubiquitination of ATG1a was enhanced in wild-type plants, attenuated in *pub25 pub26*, while increased in *PUB25/PUB26* overexpression lines (Fig. 3c). These results demonstrate that PUB25 and PUB26 directly ubiquitinate ATG1a in vitro and in vivo.

We next examined whether PUB25/PUB26 mediates ATG1a degradation. Cell-free degradation assays showed that MBP-ATG1a degraded more slowly in *pub25 pub26* protein extracts and more rapidly in extracts from *PUB25/PUB26* overexpression lines compared with wild type (Fig. 3d and Supplementary Fig. 8a, b). This degradation was largely blocked by MG132, indicating that PUB25 and PUB26

promote ATG1a turnover via the 26S proteasome. Previous studies have shown that ATG1 proteins undergo proteasomal degradation after starvation, particularly during prolonged starvation[6,8,26], Consistent with these reports, we observed that ATG1a levels declined after extended nitrogen starvation (≥ 36 h) in wild-type plants. This decline was delayed in *pub25 pub26* (Fig. 3e, f) and accelerated in *PUB25/PUB26* overexpression lines (Supplementary Fig. 8c, d), indicating that *PUB25/PUB26* promotes ATG1a turnover during prolonged nitrogen starvation.

To determine whether reduced ATG1 accumulation contributes to the impaired autophagy in *PUB25/PUB26* overexpression lines, we introduced *35S::YFP-ATG1a* to elevate ATG1 protein levels (Supplementary Fig. 8e). This transgene restored autophagy activity (Supplementary Fig. 8f) and rescued the hypersensitivity to nitrogen starvation in *PUB25/PUB26* overexpression lines (Fig. 3g, h, and Supplementary Fig. 8g, h). Thus, PUB25 and PUB26 negatively regulate nitrogen starvation-induced autophagy by controlling ATG1a stability.

Nitrogen starvation induces phosphorylation of PUB25/PUB26 at Thr95/Thr94

To investigate how PUB25 and PUB26 regulate starvation-induced autophagy, we examined the effect of nutrient deprivation on their expression. qRT-PCR analysis showed that *PUB25/PUB26* transcript levels were downregulated under both carbon and nitrogen starvation (Supplementary Fig. 9a, b). We next analyzed PUB25 and PUB26 proteins under nitrogen starvation. Both PUB25 and PUB26 migrated as two distinct bands, with the slower-migrating band increasing in a time-dependent manner upon nitrogen starvation (Fig. 4a, b), an effect not observed under nitrogen-replete conditions (Supplementary Fig. 9c-e) and independent of the epitope tag (Supplementary Fig. 9f, g). This slower-migrating band was sensitive to λ-phosphatase treatment (Fig. 4c and Supplementary Fig. 9h), indicating that it represents a

phosphorylated form of PUB25/PUB26. Thus, PUB25/PUB26 exists in both phosphorylated and non-phosphorylated states in planta, with nitrogen starvation promoting its phosphorylation. In contrast, their phosphorylation levels decreased upon fixed-carbon starvation (Supplementary Fig. 9i-k).

To identify the phosphorylation sites induced by nitrogen starvation, we performed LC-MS/MS analysis on PUB26-MYC isolated from nitrogen-deprived *pub25 pub26* expressing *proPUB26::PUB26-MYC*. Increased phosphorylation of Thr94, Ser406, and Ser410 was detected in PUB26, with corresponding conserved residues in PUB25 identified as Thr95, Ser405, and Ser409 (Fig. 4d, e and Supplementary Fig. 10a-c). Thr94 lies in the flexible linker between the U-box and ARM domains, whereas Ser406 and Ser410 are located in the C-terminal region adjacent to the ARM domain (Fig. 4e). To assess the functional relevance of these sites, we introduced alanine (A; phospho-null) and aspartic acid (D; phospho-mimic) substitutions at each site and expressed the mutants under the native promoter in *pub25 pub26*. Nitrogen starvation-induced phosphorylation was largely abolished in PUB25$^{T95A/T95D}$ and PUB26$^{T94A/T94D}$ mutants, whereas phosphorylation levels in PUB26$^{S406A/S406D}$ and PUB26$^{S410A/S410D}$ mutants remained comparable to wild-type (Fig. 4f, g and Supplementary Fig. 10d, e). Combined mutations at Ser406 and Ser410 (PUB26^{2A}, S406A/S410A; PUB26^{2D}, S406D/S410D) also did not impair phosphorylation, whereas mutations including Thr94 (PUB26^{3A}, T94A/S406A/S410A; PUB26^{3D}, T94D/S406D/S410D) abolished the phosphorylation signal (Fig. 4h and Supplementary Fig. 10f), indicating that Thr94 plays a dominant role. Furthermore, using antibodies specifically recognizing phosphorylated peptides spanning PUB25 Thr95 and PUB26 Thr94 (anti-pT95/T94) confirmed enhanced phosphorylation at these residues under nitrogen deprivation (Fig. 4i). Collectively, these results establish Thr95/Thr94 as the primary phosphorylation

sites in PUB25/PUB26 induced by nitrogen starvation.

FER directly interacts with and phosphorylates PUB25 and PUB26

To identify the kinase responsible for nitrogen starvation-induced PUB25/PUB26 phosphorylation, we first examined ATG1, a known autophagy-related kinase. However, PUB26 Thr94 phosphorylation was unaltered in *atg1abct* mutants or *ATG1a* overexpressing lines under nitrogen starvation (Supplementary Fig. 11a, b). CPK28 and OST1, which are known to phosphorylate PUB25/PUB26 at Thr95/Thr94[32,34], were also not involved, as both *cpk28* and *ost1* mutants showed similar phenotypes to Col-0 under nitrogen starvation (Supplementary Fig. 11c-f). ATG8a lipidation assays showed no difference between Col-0 and *cpk28* mutants, whereas *ost1* mutant exhibited suppressed autophagy, likely due to altered ABA-TOR signaling in the mutant[52] (Supplementary Fig. 11g, h). These results suggested that a distinct kinase mediates PUB25/PUB26 phosphorylation to negatively regulate nitrogen starvation-induced autophagy.

To identify the potential kinase, we performed IP-MS using PUB26$^{80-421}$-MYC as bait and detected several candidate kinases, including FERONIA (FER), a receptor kinase previously reported to negatively regulate autophagy[46] (Supplementary Fig. 12 and Supplementary Data 1). Y2H assays revealed that the intracellular kinase domain of FER (FER-KD) directly interacts with PUB25 and PUB26 primarily through the C-terminal region of PUB25/PUB26 (Fig. 5a, b). This direct interaction was further confirmed by GST pull-down, split-LUC, BiFC, and Co-IP assays (Fig. 5c, d, e, and Supplementary Fig. 13a), and this interaction was unaffected by nitrogen starvation (Supplementary Fig. 13b).

Given this physical interaction, we first tested whether FER serves as a ubiquitination substrate of PUB25/PUB26. Under nitrogen starvation, FER protein

accumulated, but its ubiquitination levels remained low and unchanged even upon *PUB26* overexpression (Fig. 5f and Supplementary Fig. 13c). In vitro ubiquitination assays confirmed that PUB25/PUB26 does not directly ubiquitinate the FER-KD (Supplementary Fig. 13d). The starvation-induced accumulation of FER was instead attributable to transcriptional upregulation (Fig. 5g), aligning with prior report[53]. Moreover, nitrogen starvation did not significantly alter FER phosphorylation (Supplementary Fig. 13e). Collectively, these results indicate that FER is up-regulated by nitrogen starvation, and it is not a direct ubiquitination target of PUB25/PUB26.

We then investigated whether FER phosphorylates PUB25/PUB26. In vitro kinase assays showed that HIS-FER-KD, but not the kinase-dead mutant HIS-FER^{K565R}-KD, phosphorylated GST-PUB25/PUB26 in an ATP-dependent manner, with phosphorylation reversed by λ-phosphatase (Fig. 5h and Supplementary Fig. 14a, b), confirming that FER directly phosphorylates PUB25/PUB26. IP-MS analysis of in vitro phosphorylated PUB26 identified multiple S/T residues, including Thr94, that are directly targeted by FER (Fig. 5i and Supplementary Data 2). To verify whether FER directly phosphorylates Thr95 in PUB25 and Thr94 in PUB26, we assessed FER-mediated phosphorylation of the PUB25$^{T95A/T95D}$ and PUB26$^{T94A/T94D}$ mutants. Immunoblot analysis using anti-pSer/Thr and anti-pT95/T94 antibodies revealed that phosphorylation of these mutants was markedly impaired (Fig. 5j and Supplementary Fig. 14c). In contrast, mutation of Ser406, Ser410, or both did not affect FER-dependent phosphorylation (Supplementary Fig. 14d, e). Consistently, anti-pT95/T94 antibodies detected strong phosphorylation of PUB26-FLAG affinity-purified from nitrogen-starved wild-type plants, which was reduced by the FER-specific inhibitor Reversine[54] or in the *fer-4* mutant background (Fig. 5k, l). Furthermore, although FER interacts with ATG1 family members, it did not directly phosphorylate ATG1a in vitro

(Supplementary Fig. 15). Together, these results demonstrate that nitrogen starvation-induced phosphorylation of PUB25/PUB26 at Thr95/Thr94 is primarily mediated by FER.

FER-mediated phosphorylation enhances the E3 ligase activity of PUB26 toward ATG1

To determine whether FER-mediated phosphorylation regulates PUB25/PUB26 function, we first assessed its impact on E3 ligase activity. Given that CPK28-mediated phosphorylation of PUB25 at Thr95 enhances its activity[34], we asked whether the corresponding modification at PUB26 Thr94 has a similar effect. In vitro auto-ubiquitination assays confirmed that phosphorylation at Thr94 enhanced the E3 ligase activity of PUB26 (Fig. 6a). Moreover, HIS-FER-KD markedly promoted the auto-ubiquitination of GST-PUB26, whereas the kinase-dead HIS-FER^{K565R}-KD did not (Fig. 6b), demonstrating that FER-mediated phosphorylation at Thr94 is required for the full E3 ligase activity of PUB26.

We next examined whether this phosphorylation affects PUB26-dependent ubiquitination of ATG1a. Co-expression of PUB26-MYC variants (wild-type, T94A, T94D) with YFP-ATG1a and FLAG-Ub in *pub25 pub26* protoplasts, revealed that PUB26^{T94A} was much less capable of inducing ATG1a ubiquitination than wild-type PUB26, whereas PUB26^{T94D} enhanced it (Fig. 6c). Consistently, in plants co-expressing YFP-ATG1a and PUB26-MYC variants, nitrogen starvation-induced ATG1a ubiquitination was markedly enhanced by PUB26^{T94D} (Fig. 6d). To determine whether Thr94 phosphorylation promotes ATG1a degradation during prolonged nitrogen starvation, we monitored ATG1a protein levels in *pub25 pub26* stably expressing PUB26 variants driven by its native promoter. After 36 h of nitrogen starvation, ATG1a degradation was accelerated by PUB26^{T94D} but delayed by PUB26^{T94A} compared to

PUB26 (Fig. 6e). In line with this, *fer-4* mutants exhibited reduced ATG1a polyubiquitination and increased ATG1a accumulation after prolonged nitrogen starvation (Fig. 6f, g). Collectively, these results demonstrate that FER-mediated phosphorylation of PUB26 at Thr94 enhances its E3 ligase activity to promote ATG1a degradation upon nitrogen starvation.

We further investigated how Thr94 phosphorylation enhances PUB26 E3 ligase activity. Co-IP assays revealed that nitrogen starvation-induced phosphorylation did not alter the association between PUB26 and ATG1a (Supplementary Fig. 16a). Consistently, Y2H and Co-IP analyses showed that both $PUB26^{T94A}$ and $PUB26^{T94D}$ interacted with ATG1a comparably to wild-type PUB26 (Supplementary Fig. 16b, c). Additionally, the phosphorylation status at Thr94 did not affect PUB26 subcellular distribution, dimerization, or its interaction with the E2 enzyme UBC8 (Supplementary Fig. 16d-f). These results suggest that Thr94 phosphorylation enhances the E3 ligase activity of PUB25/PUB26 through an unknown mechanism.

FER-mediated phosphorylation of PUB26 restrains nitrogen starvation-induced autophagy

We next examined autophagy in *fer-4*. Consistent with previous reports[48,53], *fer-4* plants exhibited characteristic growth defects under both nitrogen-replete and nitrogen-starved conditions, including impaired germination and abnormal cotyledon development (Supplementary Fig. 17). However, *fer-4* displayed robustly elevated autophagy even under normal growth conditions, as evidenced by increased accumulation of GFP-ATG8a-labeled autophagy bodies in the vacuole, enhanced release of free GFP from GFP-ATG8a, and elevated ATG8a lipidation. This autophagy hyperactivity was further accentuated upon nitrogen starvation (Fig. 7a-d).

Given that FER directly phosphorylates and activates PUB25/PUB26 (Fig. 5-6), we

examined the functional relevance of this phosphorylation in autophagy regulation using transgenic lines carrying either PUB26^{T94A} or PUB26^{T94D} under the native PUB26 promoter in the *pub25 pub26* background. While PUB26 fully rescued the nitrogen starvation tolerance of *pub25 pub26* mutants, PUB26^{T94A} failed to restore tolerance. Conversely, PUB26^{T94D} conferred hypersensitivity to nitrogen deprivation, phenocopying *PUB25/PUB26* overexpression lines (Fig. 7e, f and Supplementary Fig. 18a, b). Consistently, ATG8a lipidation assays revealed that PUB26^{T94D} expression led to reduced autophagy compared with wild-type *PUB26*, whereas PUB26^{T94A} maintained elevated autophagy activity (Fig. 7g). These results indicate that FER-mediated phosphorylation of PUB26 at T94 is essential for restraining nitrogen starvation-induced autophagy in Arabidopsis.

To further establish PUB25/PUB26 functions downstream of FER, we generated *pub25 pub26 fer-4* triple mutant and expressed 35S::PUB26-FLAG in *fer-4*. The triple mutant phenocopied *fer-4* in terms of nitrogen starvation sensitivity (Supplementary Fig. 18c, d), whereas *PUB25* and *PUB26* overexpression partially rescued the *fer-4* growth defect under both nitrogen-rich and nitrogen-starvation conditions (Supplementary Fig. 18e, f). Consistent with these phenotypes, ATG8a lipidation levels in *pub25 pub26 fer-4* were comparable to those in *fer-4*, but *PUB26* overexpression partially alleviated the elevated autophagy activity observed in *fer-4* (Fig. 7h, i). Collectively, these results confirmed that PUB25/PUB26 acts downstream of FER in negatively regulating nitrogen starvation-induced autophagy.

FER directly phosphorylates ATG13 to inhibit autophagy under nitrogen-replete conditions

Previous studies indicate that the *fer-4* mutant exhibits constitutively activated autophagy even under nutrient-rich conditions may due to reduced TOR activity, as

FER is required for maintaining TOR kinase activity[48,49]. However, although treatment with the TOR inhibitor AZD8055 increased autophagy in both Col-0 and *fer-4*, autophagy remained substantially higher in *fer-4* than in Col-0 (Supplementary Fig. 19a, b), indicating that additional downstream effectors of FER may exist under normal conditions to suppress autophagy. To identify such candidates, we examined published phosphoproteomic datasets and found that phosphorylation levels of multiple ATG13a phosphopeptides were reduced in the *fer-4* mutant[55,56] (Supplementary Data 3). We subsequently examined the interaction between FER and ATG13. Y2H, split-LUC, BiFC, and Co-IP assays showed that FER interacts with ATG13a and its homolog ATG13b directly, and that the C-terminal region of ATG13a primarily mediates this interaction (Fig. 8a-d and Supplementary Fig. 19c). Moreover, nitrogen starvation markedly suppressed the FER-ATG13a interaction (Fig. 8e).

We next investigated whether FER phosphorylates ATG13a. In vitro phosphorylation assays demonstrated that FER directly phosphorylates ATG13a (Fig. 8f). IP-MS analysis of in vitro phosphorylated ATG13a identified 14 Ser/Tyr residues directly phosphorylated by FER (Fig. 8g and Supplementary Data 2). Given that the dephosphorylated form of ATG13a promotes ATG1-ATG13 complex formation and activates autophagy by enhancing ATG1 binding[14], we expressed YFP-ATG13a in the *fer-4* mutant and found that the ATG1a-ATG13a interaction was constitutively elevated and significantly enhanced upon nitrogen starvation in *fer-4* compared to the wild type (Fig. 8h). Collectively, these results indicate that FER directly phosphorylates ATG13 to inhibit the ATG1-ATG13 complex assembly, restricting autophagy to a minimal basal level under normal growth conditions.

Discussion

Autophagy is a dynamic process that must be precisely tuned to fluctuating nutrient

availability. To ensure timely responses to each stimulus, rapid inactivation/degradation of autophagy proteins via a negative regulatory mechanism represents an effective strategy. Although ATG1/ULK1 is targeted for autophagy-dependent degradation in yeast, mammals, and Arabidopsis[6,57,58], the ubiquitin-proteasome pathway also plays a pivotal role in regulating its turnover[6,20-23]. The Arabidopsis genome contains over 1,500 genes encoding E3 ubiquitin ligases[59]; however, to date, only the RING-type E3 ligases SINATs have been implicated in the regulation of autophagy in plants[8,60]. Here, we identify two homologous U-box E3 ligases, PUB25 and PUB26, that negatively regulate autophagy by promoting ATG1 degradation via ubiquitination under nitrogen starvation.

A previous study noted that Arabidopsis PUB25/PUB26 forms punctate structures in protoplast cells, yet their functional identity remains uncharacterized[35]. Our data show that these puncta extensively colocalize with the autophagosome marker ATG8a (Fig. 2g), indicating direct association of PUB25/PUB26 with autophagy structures. In line with this localization, we found that PUB25 and PUB26 directly interact with ATG1 and function as negative regulators of nitrogen starvation-induced autophagy (Fig. 1 and 2). We further demonstrate that PUB25/PUB26 ubiquitinates ATG1 and promote its degradation, thereby restricting autophagy activity under nitrogen starvation (Fig. 3). These findings establish PUB25/PUB26 as previously uncharacterized E3 ligases that target the ATG1 complex in plants, though the precise ubiquitination sites on ATG1 and whether PUB25/PUB26 preferentially recognizes active ATG1 warrant further investigation. We also note that the PUB25 and PUB26 puncta display size heterogeneity similar to other plant PUB proteins[61-63], suggesting they may dynamically associate with other endomembrane compartments.

Further study revealed that nitrogen starvation induces phosphorylation of

PUB25/PUB26 at Thr95/Thr94 residue (Fig. 4). This regulatory pattern aligns with previous reports that most plant U-box E3 ubiquitin ligases are phosphorylated in response to environmental stimuli[31,64-67,68], indicating that phosphorylation serves as a conserved mechanism for this family to sense and transduce external signals. Notably, the receptor kinase FER was previously shown to directly phosphorylate and activate the E3 ubiquitin ligase ATL6 under carbon/nitrogen imbalance[53]. Consistent with this notion, we further demonstrated that FER directly interacts with and phosphorylates PUB25/PUB26 at Thr95/Thr94, thereby enhancing their E3 ubiquitin ligase activity to promote ATG1 degradation upon nitrogen starvation (Fig. 5, 6). Further genetic evidence supports that FER acts upstream of PUB25/PUB26 to negatively regulate autophagy (Fig.7 and Supplementary Fig. 18). Notably, overexpression of the wild-type *PUB26* partially alleviates the robust autophagy in *fer-4* (Fig. 7i) and partially rescues its germination and growth defects (Supplementary Fig. 18e, f). These observations suggest that accumulation of PUB26 protein may compensate for the loss of FER-mediated activation (likely via basal Thr94 phosphorylation), and that the uncontrolled robust autophagy in *fer-4* is detrimental to plants, highlighting that PUB25/PUB26 may function as guard against excessive autophagy.

It is interesting that the Thr95/Thr94 phosphorylation of PUB25/PUB26 identified under nitrogen starvation is also targeted by CPK28 and OST1 during plant immunity and cold stress responses[32,34]. These distinct kinases (CPK28, OST1, FER) phosphorylate the same conserved Thr95/Thr94 site of PUB25/PUB26, yet direct the degradation of pathway-specific substrates, BIK1 in immunity, MYB15 in cold acclimation, and ATG1 in nitrogen starvation. This convergence of multiple upstream inputs onto a single phospho-acceptor residue represents a broadly conserved signaling strategy across eukaryotes, exemplified by key mammalian signaling proteins including

451 the tumor suppressor p53 and the cAMP response element-binding protein (CREB)[69,70],
452 as well as by the plant regulator of G-protein signaling 1 (AtRGS1)[71,72]. Consistent with
453 prior studies[32,34], we demonstrate phosphorylation at Thr95/Thr94 specifically
454 enhances the E3 ligase activity of PUB25/PUB26. These residues lie in the flexible
455 linker between the U-box catalytic domain and ARM substrate-binding domain, and are
456 highly conserved among Class IV U-box proteins (PUB20/21/22/23/24/25/26)[34,73,74].
457 Unlike PUB22-Thr88, which regulates PUB22 protein stability[73], Thr94
458 phosphorylation does not affect PUB26 stability (Fig. 4), nor does it alter substrate
459 binding, localization, dimerization, or E2 interaction (Supplementary Fig. 16). Thus,
460 Thr95/Thr94 phosphorylation enhances E3 activity of PUB25/PUB26 likely via the
461 induction of conformational changes similar to mammalian HECT E3 ligases[75,76],
462 though direct structural evidence remains lacking.

463 TOR kinase is well established to hyperphosphorylate ATG13 under nutrient-
464 replete conditions to prevent ATG1-ATG13 complex formation, thereby suppressing
465 autophagy across eukaryotes[13,77]. Although FER was previously thought to regulate
466 autophagy primarily through maintaining TOR activity[10,46,48]. Our findings reveal that
467 it also represses autophagy through additional, partially TOR-independent pathways
468 (Supplementary Fig. 19a, b). Specifically, beyond regulating PUB25/PUB26, FER
469 directly phosphorylates ATG13 to impair its interaction with ATG1, thereby restraining
470 autophagy initiation under nitrogen-rich conditions (Fig. 8). These results suggest that,
471 like TOR, FER can directly modulate ATG13 phosphorylation. Whether the two kinases
472 target overlapping or distinct sites on ATG13, and whether they act synergistically or
473 redundantly, remain to be determined. In yeast and mammals, ATG13 is phosphorylated
474 by multiple other kinases independent of TOR, including the cAMP-dependent protein
475 kinase (PKA), AMP-activated kinase (AMPK), and cyclin-dependent kinase 1

476 (CDK1)[78-80]. Our study identifies FER as the first non-TOR kinase in plants directly
477 shown to phosphorylate ATG13, suggesting that the use of multiple upstream kinases
478 to fine-tune ATG13 phosphorylation represents an evolutionarily conserved strategy
479 across eukaryotes.

480 Consistent with this multilayered phosphorylation control, our previous work has
481 demonstrated that TOPP phosphatases mediate ATG13 dephosphorylation at a
482 minimum of 18 amino acid sites[14], several of which partially overlap with the FER-
483 dependent phosphorylation sites identified in this study. This indicates that FER and
484 TOPP likely act antagonistically to shape the phosphorylation dynamics of ATG13,
485 thereby ensuring tight and reversible control over autophagy initiation. Intriguingly, the
486 FER-ATG13 interaction is diminished upon nitrogen starvation despite increased FER
487 abundance (Fig. 8e and Fig. 6f). Given that starvation triggers global dephosphorylation
488 of ATG13[6,14,26], this reduction in interaction suggests that the binding affinity of FER
489 for ATG13 may depend, at least in part, on the phosphorylation status of ATG13.

490 An unexpected finding is that PUB25/PUB26 negatively regulates nitrogen
491 starvation-induced autophagy but positively regulates carbon starvation-induced
492 autophagy (Supplementary Fig. 3 and 4). It is increasingly recognized that carbon and
493 nitrogen starvation have different impacts on autophagy[9,81]. For example, while
494 nitrogen starvation acts primarily through the canonical ATG1-dependent route to
495 induce general autophagy, prolonged carbon starvation can activate an alternative,
496 ATG1-independent pathway that relies instead on SnRK1-mediated phosphorylation of
497 ATG6[9]. Given that PUB25/PUB26 directly interacts with ATG6 (Supplementary Fig. 6)
498 and this SnRK1-ATG6 axis operates under carbon starvation, we speculate that
499 PUB25/PUB26 may positively regulate carbon starvation-induced autophagy by
500 directly modulating ATG6. In addition, carbon starvation is routinely induced by

prolonged sucrose-free dark treatment, which concomitantly activates light-dark transition signaling networks, adding additional regulatory complexity to autophagy responses[82]. Notably, carbon starvation induces dephosphorylation of PUB25/PUB26, in contrast to the phosphorylation observed under nitrogen deficiency (Supplementary Fig. 9i-k). This nutrient-dependent, phosphorylation-driven functional switching of a single E3 represents an economical and exquisite strategy, enabling plants to dynamically adapt to complex and fluctuating nutritional conditions.

In conclusion, this work establishes two previously uncharacterized negative regulatory pathways modulating ATG1-ATG13 kinase complex activity in plants. Under nitrogen-rich conditions, FER, together with TOR kinase, interacts with and phosphorylates ATG13, blocking ATG1-ATG13 complex assembly. Meanwhile, FER sustains minimal phosphorylation of PUB25/PUB26 to maintain basal ATG1 turnover. These mechanisms collectively maintain autophagy at a low basal level. Upon nitrogen starvation, TOR kinase is rapidly inactivated by upstream regulators such as SnRK1, and the FER-ATG13 interaction is disrupted (likely due to ATG13 dephosphorylation), relieving the inhibitory effect to promote ATG1-ATG13 complex formation and autophagy initiation. As nitrogen deprivation persists, FER is transcriptionally upregulated and accumulates. The enhanced FER-mediated phosphorylation at Thr95/Thr94 amplifies PUB25/PUB26 E3 ligase activity, accelerating ATG1 ubiquitination and degradation to restrain ATG1-ATG13 reassembly. These events constitute an inducible attenuation mechanism to fine-tune the magnitude of autophagy to appropriate cellular levels during prolonged nitrogen starvation (Fig. 8i). Collectively, our study reveals a sophisticated, biphasic negative regulatory mechanism that precisely modulates autophagy activity according to variable nitrogen status, thereby ensuring cellular homeostasis during nutrient fluctuations.

Methods

Plant materials and growth conditions

All materials used in this work were Arabidopsis accession Columbia (Col-0). Mutants of *atg5-1* (SAIL_129_B07), *atg7-3* (SAIL_11_H07), *pub25* (SALK_147032C), and *pub26* (SALK_00174C) were obtained from the Arabidopsis Biological Resource Center (ABRC). The *atg13ab* and *atg1abct* mutants[6,9], the *pub25 pub26* double mutant[32], the *ost1-3* (SALK_008068) mutant[83], and the *cpk28* (SALK_112540) mutant[84] are well characterized in published studies. The transgenic line *proATG8a::GFP-ATG8a*/Col-0 was described in an earlier study[85]. The *fer-4* (GABI_GK106A06) mutant and *proFER::FER-GFP*/*fer-4* transgenic line have been described previously[86]. Other stable expression transgenic plants were generated in this study and listed in Supplementary Data 4. Arabidopsis seedlings were surface-sterilized and vernalized at 4℃ for 2 to 3 d, then germinated on 1/2 MS medium at 22℃ under an LD photoperiod (16 h light/8 h darkness) with illumination at ~100 μmol m^{-2} s^{-1}. After 1 week, the seedlings were transferred to soil for further growth. *N. benthamiana* was grown under LD conditions. One-month-old tobacco plants were used for transient expression assays.

Fixed carbon and nitrogen starvation treatment

The effects of fixed-carbon starvation on plant growth and survival were determined as described[14]. For nitrogen starvation, 7-day-old seedlings grown on 1/2 MS medium for 7 days were transferred to a nitrogen-free liquid medium and cultured for 5-6 days to observe phenotypes. Alternatively, sterilized and vernalized seeds were directly sown on nitrogen-free solid medium to observe the growth.

Measurement of chlorophyll contents

The sample was ground into a powder, mixed with 500 μL of 95% ethanol, and

incubated in the dark at 4°C overnight. The mixture was then centrifuged at 14,000 rpm for 10 minutes at 4°C to separate the supernatant from the tissue debris. The absorbance of the supernatant was measured at wavelengths of 649 nm and 665 nm, and the chlorophyll content was calculated as described previously[48,82].

Plasmid construction

All gene-specific primers are listed in Supplementary Data 4. Plasmids were constructed primarily using the Gateway Cloning Kit (Thermo Fisher Scientific) or the ClonExpress II One Step Cloning Kit (Vazyme, C112-02). Site-directed mutagenesis of PUB25/PUB26 was performed by PCR using mutagenic primers and pDONR-PUB25/PUB26 as the template, followed by DpnI digestion of the template and transformation into *E. coli*. All constructed plasmids used in this study are listed in Supplementary Data 4.

Concanavalin A treatment and confocal laser scanning microscopy

For concanavalin A (ConcA) (Sigma, C9705) treatment, Arabidopsis seedlings expressing GFP or YFP reporters were grown on 1/2 MS medium for 5 d, then transferred to nitrogen-free liquid medium with or without 0.5 μM ConcA for 6–8 h. Following incubation, the GFP/YFP-labeled autophagosomes in the roots were visualized with a ZEISS LSM880 confocal laser scanning microscope, using 40 × water objectives. Excitation was performed at 488 nm, and emission was collected at 500–540 nm for GFP signal. Three to four representative images in the root elongation zone were photographed per seedling, and the number of GFP-ATG8a puncta in each image was counted and averaged. A total of ten seedlings were observed per treatment. Identical settings were used for imaging of *N. benthamiana* leaf sections subjected to *A. tumefaciens*-mediated infiltration as described above.

Mass spectrometry analysis

To prepare samples for mass spectrometry analysis, at least 2 g 7-day-old seedlings of *proPUB26::PUB26-MYC/pub25 pub26* were collected. PUB26-MYC was immunoprecipitated as described above, and 50 μL of concentrated immunoprecipitate was separated by SDS-PAGE. Gels were stained with G-250, and then the PUB26-MYC bands were excised. In-gel tryptic digestion and mass spectrometry analysis were performed as described[87]. The samples were analyzed by an Ultra-high resolution liquid chromatography-mass spectrometer (Thermo Q Exactive HF-X). The software Thermo Proteome Discoverer 2.4 (Thermo Fisher Scientific) was used for data analysis.

Y2H assays

For direct protein-protein interaction by Y2H, pairwise AD and BD were co-transformed into the yeast strain Y2H Gold (Clontech). Cells transformed with both plasmids were selected after growth for 2 d at 30℃ on synthetic dropout medium lacking leucine and tryptophan (DDO). Protein-protein interactions were then identified by growing for 2 d at 30℃ on synthetic dropout medium lacking adenine, leucine, tryptophan, and histidine (QDO), or on synthetic dropout medium lacking leucine, tryptophan, and histidine (TDO) supplemented with 3-aminotriazole (3-AT).

BiFC and split-LUC

In planta protein-protein interactions were assayed using bimolecular fluorescence complementation and split-LUC in *N. benthamiana* leaves. The resulting plasmids were introduced into *A. tumefaciens* strain GV3101. Overnight cultures were resuspended in 5 mL infiltration buffer (0.15 M acetosyringone diluted in DMSO; 0.01 M MES, pH 7.5; 0.01 M $MgCl_2$), incubated at room temperature for 4 h in the darkness, and then used for direct infiltration of 4 to 6-week-old *N. benthamiana* leaves. For BiFC analysis, leaf sections of approximately 2 mm × 2 mm excised 36–48 h after infiltration were visualized using a Leica DMi8 fluorescence microscope with 20 × objectives. For split-

LUC, the assay was performed as previously described[88], the images were captured by CCD.

Transient expression in Arabidopsis protoplasts

Transient expression assays in Arabidopsis protoplasts were conducted essentially as described previously[89]. Subcellular localization was subsequently examined using a ZEISS LSM880 confocal laser scanning microscope, with 40 × water objectives. The following excitation and emission settings were used: for GFP, 488 nm excitation and 500–540 nm emission; for RFP, 561 nm excitation and 580–620 nm emission; for chloroplast autofluorescence, 640 nm excitation and 650–750 nm emission.

Protein isolation and immunoblot analysis

For protein extraction, Arabidopsis samples were ground and homogenized in ice-cold extraction buffer (10 mM HEPES, pH 7.5; 100 mM NaCl; 1 mM EDTA, pH 8.0; 10% Glycerol; 0.5% Triton X-100; 1 × cocktail). Samples were incubated on ice for 10–15 min and centrifuged at 4℃ for 10 min at 12,000 *g*. The supernatant was used for electrophoresis. For immunoblot analysis, total proteins were subjected to SDS-PAGE and electrophoretically transferred to a polyvinylidene fluoride membrane (Immobilon-P; Millipore). For ATG8a assay, total protein was separated by SDS-PAGE in the presence of 6 M urea. Antibodies used in the protein blotting analysis were ATG1a (Agrisera, AS194274, 1:3000), ATG8a (Agrisera, AS142769, 1:2000), GFP (Abmart, M20004, 1:5000), FLAG (Abmart, 80010-1-RR, 1:5000), GST (Abmart, M20007, 1:5000), MBP (Abmart, 15089-1-AP, 1:5000), HIS (Abmart, M2000S, 1:5000), MYC (Abmart, M20002S, 1:5000), β-Actin (CWBIO, CW0264, 1:5000), pSer/Thr (Abcam, ab17464, 1:5000), Phospho-PUB25/PUB26 (T95/T94) (P26167, Abmart, 1:5000), UBQ11 (Agrisera, AS08307A, 1:10000).

Recombinant protein expression and pull-down

For the expression of recombinant protein in prokaryotic cells, the CDSs of PUBs were cloned into the pGEX-4T-1 (GST tag) vector and transformed into the *E. coli* strain *Rosetta*. GST-tagged proteins were purified with Glutathione Sepharose 4B beads (GE Healthcare, 10250335). The CDSs of ATG1a and ATG13a were cloned into the pMAL-c2x (MBP tag) vector and transformed into the *E. coli s*train *Rosetta*. MBP-tagged proteins were purified using PurKine™ MBP-Tag Dextrin Resin 6FF (Abbkine, BMR20206) following the manufacturer's instructions. For HIS-FER-KD and HIS-FER^{K565R}-KD expression, the CDSs of FER-KD and FER^{K565R}-KD were cloned into the pET28a (HIS tag) vector, with GST-ABI2 (acting as helper) co-expressed in BL21 (DE3) codon plus (Weidi, EC1007). His-tagged proteins were purified with Ni-NTA Beads (Smart-lifesciences, SA005005) following the instructions. Protein concentration was determined using the BCA protein assay kit (Abbkine, KTD3001). In vitro pull-down assay was performed as described[14].

Co-IP

For Co-IP in Arabidopsis, 7-day-old seedlings of Col-0 co-expressing PUB25/PUB26-FLAG and YFP-ATG1a or FER-GFP were ground in liquid nitrogen and homogenized in ice-cold IP buffer (10 mM HEPES, pH 7.5; 100 mM NaCl; 1 mM EDTA, pH 8.0; 10% Glycerol; 0.5% Triton X-100; 1 × cocktail). Samples were incubated on ice for 10–15 min and centrifuged at 4℃ for 10 min at 12,000 *g*. The supernatant was then incubated with anti-GFP nanobody agarose beads (AlpalifeBio, KTSM1334) for 2 h at 4℃ to immunoprecipitate the target protein. The beads were collected and washed with cold IP buffer 3–5 times.

For Co-IP in tobacco, constructs of *35S:: PUB-MYC* and *35S::YFP-ATG1a* were infiltrated into *N. benthamiana* via the *Agrobacterium*-mediated method. After 48 h, total proteins were extracted with IP buffer (50 mM Tris-HCl, pH 7.5; 150 mM NaCl;

5 mM dithiothreitol; 1% Triton X-100; 2% NP40 and 1 × cocktail) followed by incubating with anti-MYC nanobody agarose beads (AlpalifeBio, KTSM1336) for 2 h. Beads were washed 6–8 times with washing buffer (50 mM Tris-HCl, pH 7.5; 150 mM NaCl; 1% Triton X-100; 2% NP40). The immunoprecipitated proteins were analyzed by SDS-PAGE and immunoblotted with GFP antibody.

Cell-free assay

Take 200-400 mg of 7-day-old normally grown plants and extract total proteins using protein degradation buffer (50 mM Tris-HCl, pH 7.5; 100 mM NaCl; 5 mM DTT; 5 mM ATP). Add 100 ng of purified MBP-ATG1a protein and incubate at room temperature for 0, 5, 15, 30, and 60 minutes. Collect equal amounts of the reaction mixture at each time point to detect MBP-ATG1a expression. Actin were used as loading controls. Additionally, 5 μM MG132 (MedChemExpress, HY-13259) was added to the indicated samples to examine protein degradation through the 26S proteasome pathway.

In vitro and in vivo ubiquitination assay

Add 1.2 μg of substrate protein MBP-ATG1a or HIS-FER-KD, 100 ng UBE1 (Ubbiotech, UBE-024), 200 ng UBCH5 (Ubbiotech, UBE-622), 800 ng GST-PUB25/PUB26, and 2 μg ubiquitin FLAG-Ub (Boston Biochem, U-120) to the in vitro ubiquitination reaction buffer (100 mM Tris-HCl pH 7.5; 25 mM $MgCl_2$; 2.5 mM DTT; 10 mM ATP). Incubate the mixture at 37°C for the indicated times. The reaction was terminated by adding 5 × protein loading buffer and boiling at 100 °C for 5 min. The sample was separated by SDS-PAGE and detected by immunoblot using anti-HIS, anti-GST, anti-MBP, and anti-FLAG antibodies.

To test the ubiquitination of ATG1a in vivo, *pub25 pub26* mutant protoplasts were transfected with plasmids combination of FLAG-Ub, YFP-ATG1a, and PUB26-MYC

varieties (PUB26, PUB26^{T94A}, PUB26^{T94D}) or controls with 5 μM MG132. The cells were then lysed with the extraction buffer (50 mM HEPES, pH 7.5; 150 mM NaCl; 2 mM DTT; 1% Triton X-100; 1 × EDTA-free protease inhibitor cocktail), and the total proteins were immunoprecipitated with FLAG beads. The ubiquitination of ATG1a was detected with anti-GFP antibody.

In vitro and in vivo phosphorylation assay

For the in vitro phosphorylation assay, 0.5 μg purified HIS-FER-KD and the kinase-dead mutant HIS-FER^{K565R}-KD proteins were co-incubated with 2.5 μg GST-PUB25/PUB26 in phosphorylation reaction buffer (25 mM Tris-HCl, pH 7.5; 1 mM $MnCl_2$; 10 mM $MgCl_2$; 1 mM DTT; 1 mM ATP) at 30°C for 30 minutes. Anti-pSer/Thr antibody (Abcam, ab17464, 1:5000) and anti-Phospho-PUB25/PUB26 (T95/T94) (P26167, Abmart, 1:5000) were used to detect phosphorylation signal. To test the protein phosphorylation of PUB-MYC or PUB-FLAG expressed in Arabidopsis after nutrient starvation, samples were lysed with the extraction buffer (100 mM Tris-HCl, pH 6.8; 4% SDS; 1.43% β-Mercaptoethanol; 20% Glycerol) followed by incubating with anti-MYC or anti-FLAG beads. Anti-Phospho-PUB25/PUB26 (Thr95/Thr94) was used to detect phosphorylation signal.

RNA extraction and qRT-PCR analysis

RNA extraction was performed according to the instructions of the total RNA kit (Accurate Biology, AG21019). Evo M-MLV RT Kit with gDNA Clean (Accurate Biology, AG11705) was used to synthesize cDNA. qRT-PCR analysis was performed using SYBR Green Pro Taq HS (Accurate Biology, AG11718) and the QuantStudio5 PCR instrument. *Ubiquitin10* (*UBQ10*) was used as a reference gene. The gene-specific primers used for qRT-PCR are listed in Supplementary Data 4.

Statistical analysis

All graphs were generated using GraphPad Prism 8.0 software. Data are presented as mean ± SD. Statistical differences were determined using one-way ANOVA followed by Tukey's post hoc test (for multiple comparisons) or unpaired two-tailed Student's *t* test. All analyses were performed using IBM SPSS Statistics 22 or Excel. Detailed information about statistical analysis is provided in the figure legends. The *P* value < 0.05 was considered statistically significant.

Reporting summary

Further information on research design is available in the Nature Portfolio Reporting Summary linked to this article.

Data availability

The main data supporting the findings of this study are contained within the article and its Supplementary Figures. All uncropped original western blot (WB) gel images, as well as the raw data of the relevant statistics presented in main Figures 1-8 and Supplementary Figures 1-19, are provided as a Source Data file. The Source Data have been submitted together with this article.

Reference

1. Yagyu, M. & Yoshimoto, K. New insights into plant autophagy: molecular mechanisms and roles in development and stress responses. *J. Exp. Bot.* **75**, 1234-1251 (2024).
2. Gross, A.S., Raffeiner, M., Zeng, Y., Üstün, S. & Dagdas, Y. Autophagy in plant health and disease. *Annu. Rev. Plant Biol.* **76**, 197-227 (2025).
3. Zhuang, X., Li, B. & Jiang, L. Autophagosome biogenesis and organelle homeostasis in plant cells. *Plant Cell* **36**, 3009-3024 (2024).
4. Mizushima, N. The role of the Atg1/ULK1 complex in autophagy regulation. *Curr. Opin. Cell Biol*. **22**, 132-139 (2010).

5. Wang, Q. & Hou, S. The emerging roles of ATG1/ATG13 kinase complex in plants. *J. Plant Physiol*. **271**, 153653 (2022).
6. Suttangkakul, A., Li, F., Chung, T. & Vierstra, R.D. The ATG1/ATG13 protein kinase complex is both a regulator and a target of autophagic recycling in Arabidopsis. *Plant Cell* **23**, 3761-3779 (2011).
7. Li, F., Chung, T. & Vierstra, R.D. AUTOPHAGY-RELATED11 plays a critical role in general autophagy- and senescence-induced mitophagy in Arabidopsis. *Plant Cell* **26**, 788-807 (2014).
8. Qi, H. et al. Arabidopsis SINAT proteins control autophagy by mediating ubiquitylation and degradation of ATG13. *Plant Cell* **32**, 263-284 (2019).
9. Huang, X. et al. Genetic analyses of the Arabidopsis ATG1 kinase complex reveal both kinase-dependent and independent autophagic routes during fixed-carbon starvation. *Plant Cell* **31**, 2973-2995 (2019).
10. Schumacher, K., Liu, Y. & Bassham, D.C. TOR is a negative regulator of autophagy in Arabidopsis thaliana. *PLoS One* **5**, e11883 (2010).
11. Soto-Burgos, J. & Bassham, D.C. SnRK1 activates autophagy via the TOR signaling pathway in Arabidopsis thaliana. *PLoS One* **12**, e0182591 (2017).
12. Chen, L. et al. The AMP-activated protein kinase KIN10 is involved in the regulation of autophagy in Arabidopsis. *Front. Plant Sci.* **8**, 1201 (2017).
13. Son, O., Kim, S., Kim, D., Hur, Y.S., Kim, J. & Cheon, C.I. Involvement of TOR signaling motif in the regulation of plant autophagy. *Biochem. Biophys. Res. Commun*. **501**, 643-647 (2018).
14. Wang, Q. et al. Type one protein phosphatase regulates fixed-carbon starvation-induced autophagy in Arabidopsis. *Plant Cell* **34**, 4531-4553 (2022).
15. Chen, R.H., Chen, Y.H. & Huang, T.Y. Ubiquitin-mediated regulation of

751 autophagy. *J. Biomed. Sci.* **26**, 80 (2019).
752 16. Wu, Y., Chen, Y., Tian, X., Shao, G., Lin, Q. & Sun, A. Ubiquitination regulates
753 autophagy in cancer: simple modifications, promising targets. *J. Transl. Med.*
754 **22**, 985 (2024).
755 17. Nazio, F. et al. mTOR inhibits autophagy by controlling ULK1 ubiquitylation,
756 self-association and function through AMBRA1 and TRAF6. *Nat. Cell Biol*. **15**,
757 406-416 (2013).
758 18. Di Rienzo, M. et al. Autophagy induction in atrophic muscle cells requires
759 ULK1 activation by TRIM32 through unanchored K63-linked polyubiquitin
760 chains. *Sci. Adv.* **5**, eaau8857 (2019).
761 19. Antonioli, M. et al. AMBRA1 interplay with cullin E3 ubiquitin ligases
762 regulates autophagy dynamics. *Dev. Cell* **31**, 734-746 (2014).
763 20. Liu, C.C. et al. Cul3-KLHL20 ubiquitin ligase governs the turnover of ULK1
764 and VPS34 complexes to control autophagy termination. *Mol. Cell* **61**, 84-97
765 (2016).
766 21. Nazio, F. et al. Fine-tuning of ULK1 mRNA and protein levels is required for
767 autophagy oscillation. *J. Cell Biol.* **215**, 841-856 (2016).
768 22. Yang, Y. et al. TRIM27 cooperates with STK38L to inhibit ULK1-mediated
769 autophagy and promote tumorigenesis. *EMBO J.* **41**, e109777 (2022).
770 23. Lee, D.E. et al. NEDD4L downregulates autophagy and cell growth by
771 modulating ULK1 and a glutamine transporter. *Cell Death Dis.* **11**, 38 (2020).
772 24. Chu, Y. et al. LUBAC and OTULIN regulate autophagy initiation and
773 maturation by mediating the linear ubiquitination and the stabilization of ATG13.
774 *Autophagy* **17**, 1684-1699 (2021).
775 25. Lee, J., Kim, J., Shin, J., Kang, Y., Choi, J. & Cheong, H. ATG101 degradation

776 by HUWE1-mediated ubiquitination impairs autophagy and reduces survival in
777 cancer cells. *Int. J. Mol. Sci.* **22**, 9182 (2021).
778 26. Qi, H. et al. 14-3-3 proteins contribute to autophagy by modulating SINAT-
779 mediated degradation of ATG13. *Plant Cell* **34**, 4857-4876 (2022).
780 27. Trenner, J., Monaghan, J., Saeed, B., Quint, M., Shabek, N. & Trujillo, M.
781 Evolution and functions of plant U-Box proteins: from protein quality control
782 to signaling. *Annu. Rev. Plant Biol.* **73**, 93-121 (2022).
783 28. Yee, D. & Goring, D.R. The diversity of plant U-box E3 ubiquitin ligases: from
784 upstream activators to downstream target substrates. *J. Exp. Bot.* **60**, 1109-1121
785 (2009).
786 29. Zhang, Y. & Zeng, L. Crosstalk between ubiquitination and other post-
787 translational protein modifications in plant immunity. *Plant Commun.* **1**, 100041
788 (2020).
789 30. Karthik, H.N., Parmar, S., Gawande, N.D. & Sankaranarayanan, S. Multifaceted
790 roles of U-box E3 ligases in plant development. *Plant Cell Physiol.* **66**, 1123-
791 1136 (2025).
792 31. Wang, K. et al. The RLI1-OsPUB77-OsBZR3 module mediates the crosstalk
793 between phosphate starvation and brassinosteroid signaling pathways to shape
794 rice shoot architecture. *Mol. Plant* **18**, 1864-1880 (2025).
795 32. Wang, X. et al. PUB25 and PUB26 promote plant freezing tolerance by
796 degrading the cold signaling negative regulator MYB15. *Dev. Cell* **51**, 222-
797 235.e5 (2019).
798 33. Wang, X., Zhang, X., Song, C.P., Gong, Z., Yang, S. & Ding, Y. PUB25 and
799 PUB26 dynamically modulate ICE1 stability via differential ubiquitination
800 during cold stress in Arabidopsis. *Plant Cell* **35**, 3585-3603 (2023).

34. Wang, J. et al. A regulatory module controlling homeostasis of a plant immune kinase. *Mol. Cell* **69**, 493-504.e6 (2018).
35. Ma, A. et al. Verticillium dahliae effector VDAL protects MYB6 from degradation by interacting with PUB25 and PUB26 E3 ligases to enhance Verticillium wilt resistance. *Plant Cell* **33**, 3675-3699 (2021).
36. Bai, J. et al. BIK1 protein homeostasis is maintained by the interplay of different ubiquitin ligases in immune signaling. *Nat. Commun.* **14**, 4624 (2023).
37. Li, Y., Zhao, Z., Ren, W., Zheng, H., Sun, M. & Dai, S. ABA signaling is involved in the regulation of BSK1 stability mediated by the UBP24-PUB25/26 module in Arabidopsis. *Cell Rep.* **45**, 117187 (2026).
38. Li, J. et al. Plant U-box E3 ligases PUB25 and PUB26 control organ growth in Arabidopsis. *New Phytol.* **229**, 403-413 (2021).
39. Chen, W. et al. An antisense intragenic lncRNA SEAIRa mediates transcriptional and epigenetic repression of SERRATE in Arabidopsis. *Proc. Natl Acad. Sci. USA* **120**, e2216062120 (2023).
40. Wu, Y. et al. The wheat E3 ligase TaPUB26 is a negative regulator in response to salt stress in transgenic Brachypodium distachyon. *Plant Sci.* **294**, 110441 (2020).
41. Zhao, T. et al. Ubiquitin ligase VvPUB26 in grapevine promotes proanthocyanidin synthesis and resistance to powdery mildew. *Plant Physiol.* **195**, 2891-2910 (2024).
42. Lin, Z. et al. Pupylation-based proximity-tagging of FERONIA-interacting proteins in Arabidopsis. *Mol. Cell Proteomics* **23**, 100828 (2024).
43. Franck, C.M., Westermann, J. & Boisson-Dernier, A. Plant malectin-like receptor kinases: from cell wall integrity to immunity and beyond. *Annu. Rev.*

Plant Biol. **69**, 301-328 (2018).

44. Cheung, A.Y. FERONIA: A receptor kinase at the core of a global signaling network. *Annu. Rev. Plant Biol.* **75**, 345-375 (2024).

45. Ali, S., Tyagi, A., Park, S., Varshney, R.K. & Bae, H. A molecular perspective on the role of FERONIA in root growth, nutrient uptake, stress sensing and microbiome assembly. *J. Adv. Res.* **75**, 35-52 (2025).

46. Wang, P. et al. FERONIA functions through Target of Rapamycin (TOR) to negatively regulate autophagy. *Front. Plant Sci.* **13**, 961096 (2022).

47. Wang, P. et al. Integrated omics reveal novel functions and underlying mechanisms of the receptor kinase FERONIA in Arabidopsis thaliana. *Plant Cell* **34**, 2594-2614 (2022).

48. Song, L. et al. The RALF1-FERONIA complex interacts with and activates TOR signaling in response to low nutrients. *Mol. Plant* **15**, 1120-1136 (2022).

49. Pacheco, J.M. et al. Cell surface receptor kinase FERONIA linked to nutrient sensor TORC signaling controls root hair growth at low temperature linked to low nitrate in Arabidopsis thaliana. *New Phytol.* **238**, 169-185 (2023).

50. Chung, T., Phillips, A.R. & Vierstra, R.D. ATG8 lipidation and ATG8-mediated autophagy in Arabidopsis require ATG12 expressed from the differentially controlled ATG12A AND ATG12B loci. *Plant Cell* **62**, 483-493 (2010).

51. Chen, L. et al. Autophagy contributes to regulation of the hypoxia response during submergence in Arabidopsis thaliana. *Autophagy* **11**, 2233-2246 (2015).

52. Wang, P. et al. Reciprocal regulation of the TOR kinase and ABA receptor balances plant growth and stress response. *Mol. Cell* **69**, 100-112.e106 (2018).

53. Xu, G. et al. FERONIA phosphorylates E3 ubiquitin ligase ATL6 to modulate the stability of 14-3-3 proteins in response to the carbon/nitrogen ratio. *J. Exp.*

Bot. **70**, 6375-6388 (2019).

54. Liu, H.B. et al. A screening of inhibitors targeting the receptor kinase FERONIA reveals small molecules that enhance plant root immunity. *Plant Biotechnol. J.* **21**, 63-77 (2023).

55. Jiang, W. et al. FERONIA regulates salt tolerance in Arabidopsis by controlling photorespiratory flux. *Plant Cell* **36**, 4732-4751 (2024).

56. Liu, J. et al. FERONIA kinase and PP2A antagonistically regulate salt tolerance in Arabidopsis. *Curr. Biol*. **36**, 370-386.e7 (2026).

57. Nakatogawa, H. et al. The autophagy-related protein kinase Atg1 interacts with the ubiquitin-like protein Atg8 via the Atg8 family interacting motif to facilitate autophagosome formation. *J. Biol. Chem.* **287**, 28503-28507 (2012).

58. Alemu, E.A. et al. ATG8 family proteins act as scaffolds for assembly of the ULK complex: sequence requirements for LC3-interacting region (LIR) motifs. *J. Biol. Chem.* **287**, 39275-39290 (2012).

59. Shabek, N. & Zheng, N. Plant ubiquitin ligases as signaling hubs. *Nat. Struct. Mol. Biol.* **21**, 293-296 (2014).

60. Qi, H. et al. TRAF family proteins regulate autophagy dynamics by modulating AUTOPHAGY PROTEIN6 stability in Arabidopsis. *Plant Cell* **29**, 890-911 (2017).

61. Kim, J.H., Kim, M.S., Kim, D.Y., Amoah, J.N. & Seo, Y.W. Molecular characterization of U-box E3 ubiquitin ligases (TaPUB2 and TaPUB3) involved in the positive regulation of drought stress response in Arabidopsis. *Int. J. Mol. Sci.* **22**, 13658 (2021).

62. Wang, N. et al. Genome-wide identification of soybean U-Box E3 ubiquitin ligases and roles of GmPUB8 in negative regulation of drought stress response

in Arabidopsis. *Plant Cell Physiol*. **57**, 1189-1209 (2016).

63. Lim, C.J. et al. MpPUB9, a U-box E3 ubiquitin ligase, acts as a positive regulator by promoting the turnover of MpEXO70.1 under high salinity in Marchantia polymorpha. *New Phytol.* **244**, 2343-2363 (2024).

64. Chen, L., Cochran, A.M., Waite, J.M., Shirasu, K., Bemis, S.M. & Torii, K.U. Direct attenuation of Arabidopsis ERECTA signalling by a pair of U-box E3 ligases. *Nat. Plants* **9**, 112-127 (2023).

65. Zhou, J. et al. Regulation of Arabidopsis brassinosteroid receptor BRI1 endocytosis and degradation by plant U-box PUB12/PUB13-mediated ubiquitination. *Proc. Natl Acad. Sci. USA* **115**, E1906-E1915 (2018).

66. Wang, G. et al. Release of a ubiquitin brake activates OsCERK1-triggered immunity in rice. *Nature* **629**, 1158-1164 (2024).

67. Liu, J. et al. The MtDMI2-MtPUB2 negative feedback loop plays a role in nodulation homeostasis. *Plant Physiol.* **176**, 3003-3026 (2018).

68. Guo, S., Peng, Y., Qi, H., Yu, L. & Wang, Q. Phosphorylation-mediated rewiring of the plant ubiquitin system: from core machinery to ubiquitin-like modifications. *J. Exp. Bot.* https://doi.org/10.1093/jxb/eraf550 (2025).

69. Maclaine, N.J. & Hupp, T.R. The regulation of p53 by phosphorylation: a model for how distinct signals integrate into the p53 pathway. *Aging* **1**, 490-502 (2009).

70. Wu, G.Y., Deisseroth, K. & Tsien, R.W. Activity-dependent CREB phosphorylation: convergence of a fast, sensitive calmodulin kinase pathway and a slow, less sensitive mitogen-activated protein kinase pathway. *Proc. Natl Acad. Sci. USA* **98**, 2808-2813 (2001).

71. Urano, D. et al. Endocytosis of the seven-transmembrane RGS1 protein activates G-protein-coupled signalling in Arabidopsis. *Nat. Cell Biol.* **14**, 1079-

1088 (2012).

72. Tunc-Ozdemir, M., Urano, D., Jaiswal, D.K., Clouse, S.D. & Jones, A.M. Direct modulation of heterotrimeric g protein-coupled signaling by a receptor kinase complex. *J. Biol. Chem.* **291**, 13918-13925 (2016).

73. Furlan, G. et al. Changes in PUB22 ubiquitination modes triggered by MITOGEN-ACTIVATED PROTEIN KINASE3 dampen the immune response. *Plant Cell* **29**, 726-745 (2017).

74. Dou, R., Miguel, V.N., Grubb, L.E., Rana, M., Saltzman, B. & Monaghan, J. Class IV plant U-box proteins function redundantly to optimize protein accumulation of receptor-like cytoplasmic kinase BIK1. *Plant Physiol*. **198**, kiaf267 (2025).

75. Chen, Z. et al. A tunable brake for HECT ubiquitin ligases. *Mol. Cell* **66**, 345-357.e6 (2017).

76. Jiang, H., Thomas, S.N., Chen, Z., Chiang, C.Y. & Cole, P.A. Comparative analysis of the catalytic regulation of NEDD4-1 and WWP2 ubiquitin ligases. *J. Biol. Chem.* **294**, 17421-17436 (2019).

77. Díaz-Troya, S., Pérez-Pérez, M.E., Florencio, F.J. & Crespo, J.L. The role of TOR in autophagy regulation from yeast to plants and mammals. *Autophagy* **4**, 851-865 (2008).

78. Stephan, J.S., Yeh, Y.Y., Ramachandran, V., Deminoff, S.J. & Herman, P.K. The Tor and PKA signaling pathways independently target the Atg1/Atg13 protein kinase complex to control autophagy. *Proc. Natl Acad. Sci. USA* **106**, 17049-17054 (2009).

79. Puente, C., Hendrickson, R.C. & Jiang, X. Nutrient-regulated phosphorylation of ATG13 inhibits starvation-induced autophagy. *J. Biol. Chem.* **291**, 6026-6035

(2016).

80. Li, Z. et al. ULK1-ATG13 and their mitotic phospho-regulation by CDK1 connect autophagy to cell cycle. *PLoS Biol.* **18**, e3000288 (2020).

81. Kacprzak, S.M. & Van Aken, O. Carbon starvation, senescence and specific mitochondrial stresses, but not nitrogen starvation and general stresses, are major triggers for mitophagy in Arabidopsis. *Autophagy* **18**, 2894-2912 (2022).

82. Yang, C. et al. HY5-HDA9 module transcriptionally regulates plant autophagy in response to light-to-dark conversion and nitrogen starvation. *Mol. Plant* **13**, 515-531 (2020).

83. Su, H. et al. Abscisic acid signaling negatively regulates nitrate uptake via phosphorylation of NRT1.1 by SnRK2s in Arabidopsis. *J. Integr. Plant Biol.* **63**, 597-610 (2021).

84. Wang, Z. et al. Calcium-dependent protein kinases CPK21 and CPK23 phosphorylate and activate the iron-regulated transporter IRT1 to regulate iron deficiency in Arabidopsis. *Sci. China Life Sci.* **66**, 2646-2662 (2023).

85. Huang, L. et al. Autophagy regulates glucose-mediated root meristem activity by modulating ROS production in Arabidopsis. *Autophagy* **15**, 407-422 (2018).

86. Chen, J. et al. FERONIA interacts with ABI2-type phosphatases to facilitate signaling cross-talk between abscisic acid and RALF peptide in Arabidopsis. *Proc. Natl Acad. Sci. USA* **113**, E5519-5527 (2016).

87. Sun, J.L., Li, J.Y., Wang, M.J., Song, Z.T. & Liu, J.X. Protein quality control in plant organelles: current progress and future perspectives. *Mol. Plant* **14**, 95-114 (2021).

88. Chen, H. et al. Firefly luciferase complementation imaging assay for protein-protein interactions in plants. *Plant Physiol.* **146**, 368-376 (2008).

89. Peng, Y., Guo, S., Lei, B., Yu, L. & Wang, Q. Autophagy deficiency confers freezing tolerance in Arabidopsis thaliana. *BMC Plant Biol.* **25**, 994 (2025).

Acknowledgments

We thank Prof. FaQiang Li (South China Agricultural University) for the *atg1abct* mutant; Prof. Feng Yu (Hunan University) for *fer-4* mutant and *proFER::FER-GFP*/*fer-4* transgenic plant; Prof. YangLin Ding and ShuHua Yang (China Agricultural University) for *pub25 pub26* mutant; Prof. Cun Wang for the *ost1* and *cpk28* mutant (Northwest A&F University); Prof. ChunZhao Zhao for the pET28a-FER-KD and pET28a-FER^{K565R}-KD constructs (Shanghai Center for Plant Stress Biology). We are grateful to Hua Zhao and Qiong Zhang (State Key Laboratory for Crop Stress Resistance and High-Efficiency Production, Northwest A&F University) for technical assistance. This work was supported by the National Natural Science Foundation of China (No.32400246 to Q.L.W, No.32572244 to L.H.Y), Natural Science Foundation of Shaanxi Province (No.2025JC-YBMS-184 to L.H.Y), and Science and Technology Program of Yangling Demonstration Zone (No.2025CYFZ-13 to L.H.Y).

Author contributions

Q.L.W and L.H.Y designed the research; Q.L.W and S.J.G performed the majority of the experiments and data analysis. Y.S.P, N.L, T.Y.Y and T.L assisted with vector construction, plant material generation, and confocal microscopy imaging. Q.L.W, L.H.Y and S.W.H wrote the manuscript. L.H.Y supervised the project. Q.L.W and L.H.Y acquired the funding for this study.

Competing interesting

The authors declare no competing interests.

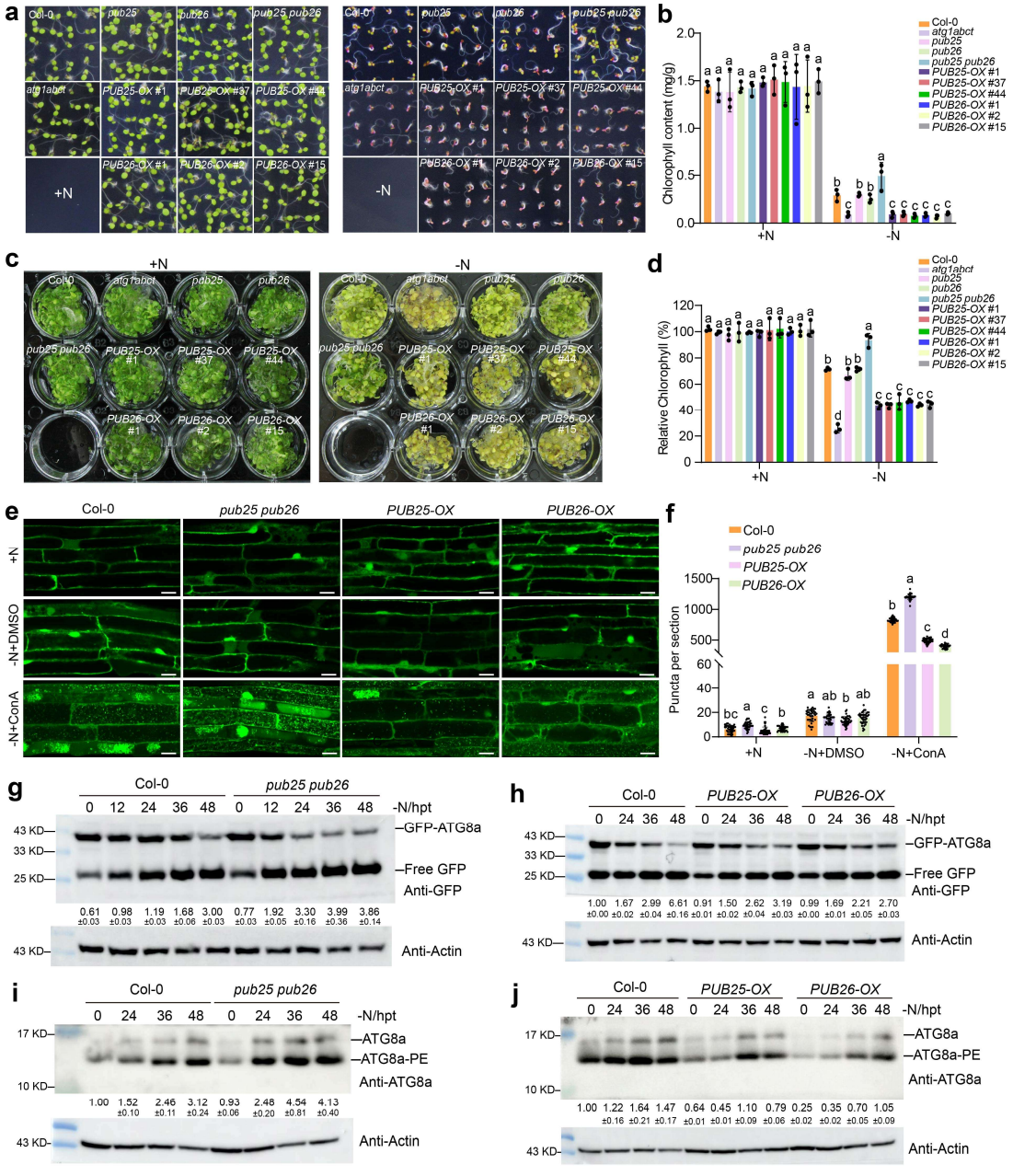

Fig. 1 | PUB25 and PUB26 negatively regulate plant tolerance to nitrogen deprivation and autophagy.

a Phenotypes of Col-0, *pub25* and *pub26* single mutants, *pub25 pub26* double mutant, and *PUB25*- or *PUB26*-overexpressing lines grown on +N or -N medium for 6 days. **b** Chlorophyll content of seedlings from (**a**). For each biological replicate, at least 64 plants were examined per genotype. Data are mean ± SD (n = 3). **c** Seedlings of the same genotypes as in (**a**) were pre-grown on +N medium for 7 days and then incubated

in -N liquid medium for 5 days. **d** Relative chlorophyll content of seedlings from (**c**), normalized to Col-0 under +N conditions (set to 100%). Data are mean ± SD (n = 3). **e** Accumulation of GFP-ATG8a-labeled autophagic bodies in the root elongation zone. Five-day-old seedlings expressing proATG8a::GFP-ATG8a were treated with or without 0.5 μM concanamycin A (ConA) under +N or -N conditions for 8 h. Scale bars, 20 μm. **f** Quantification of autophagosome puncta from (**e**). Puncta were counted in four images from the root elongation zone per seedling (10 seedlings per treatment). Data are mean ± SD (n = 40). For panels (**b, d, f**), statistical significance was determined by one-way ANOVA followed by Tukey's multiple comparison test ($P < 0.05$). Different letters denote significant differences. **g, h** Immunoblot analysis of GFP-ATG8a processing in Col-0, *pub25 pub26*, and *PUB25*- or *PUB26*-overexpressing lines under nitrogen starvation. The ratio of free GFP to GFP-ATG8a is shown below the lanes. Data are mean ± SD (n = 3). hpt, hours post-treatment. **i, j** Immunoblot analysis of ATG8a lipidation under nitrogen starvation. ATG8a-PE levels (normalized to actin) are indicated below the lanes. Data are mean ± SD (n = 3).

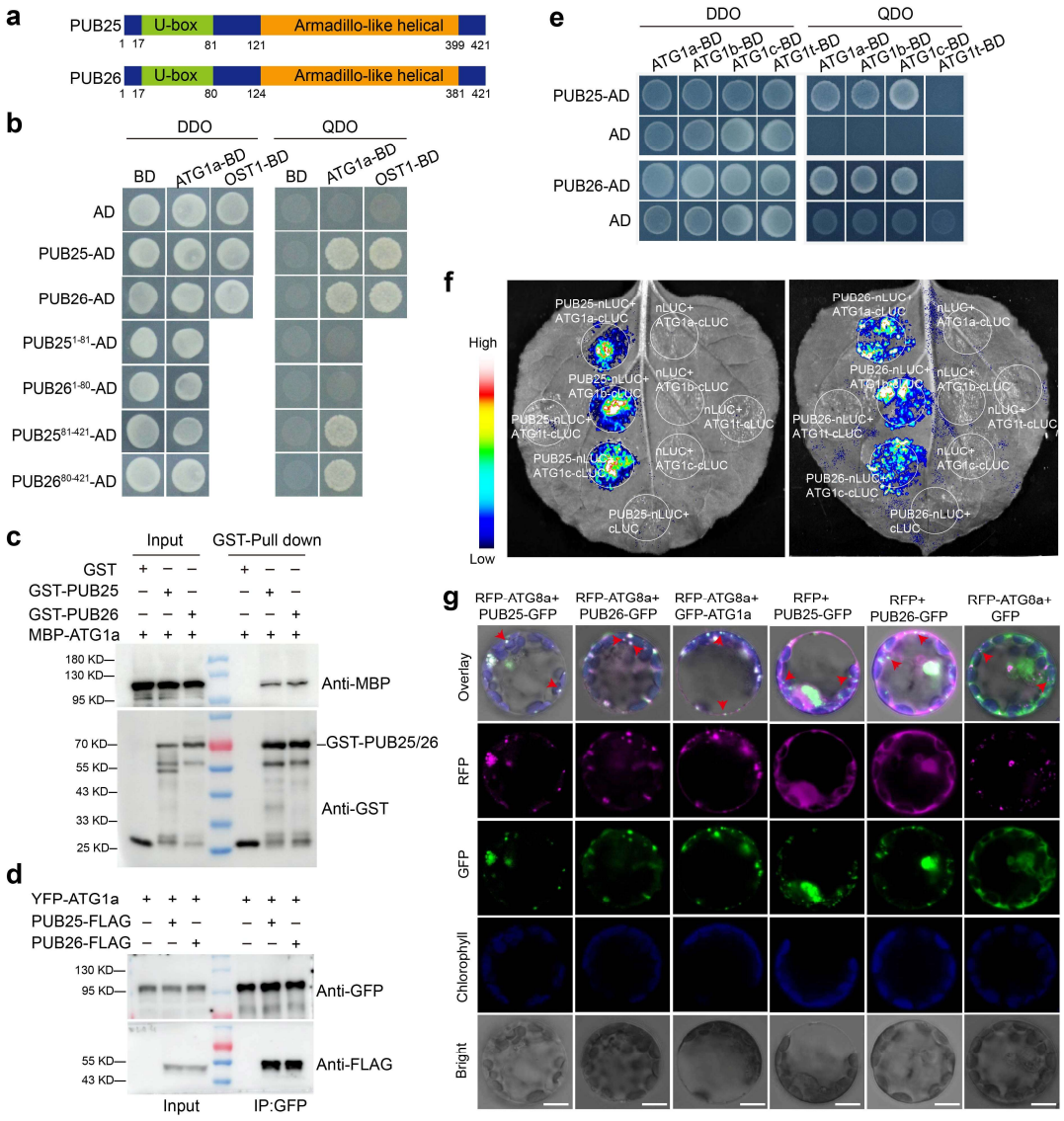

Fig. 2 | PUB25 and PUB26 directly interact with ATG1 kinase and associate with autophagosomes.

a Schematics diagrams of predicted domains in PUB25 and PUB26. **b** Direct interaction of PUB25 and PUB26 with ATG1a in yeast two-hybrid (Y2H) assays. OST1 was used as a positive control. **c** In vitro pull-down assays showing the interaction of PUB25 and PUB26 with ATG1a. **d** Co-immunoprecipitation (Co-IP) assays showing interaction of PUB25 and PUB26 with ATG1a. Total proteins from 7-day-old transgenic plants expressing YFP-ATG1a together with either PUB25-FLAG or PUB26-FLAG were immunoprecipitated with anti-GFP magnetic beads and immunoblotted with anti-

FLAG antibody. **e** Direct interaction of PUB25 and PUB26 with ATG1a, ATG1b, ATG1c, and ATG1t in Y2H assays. **f** Split-luciferin complementation imaging (Split-LUC) assays reveal that PUB25 and PUB26 interact with ATG1s. **g** Transient co-expression of PUB25-GFP and PUB26-GFP with RFP-ATG8a in Arabidopsis protoplasts. Free GFP and free RFP were used as negative controls. Scale bars, 10 μm.

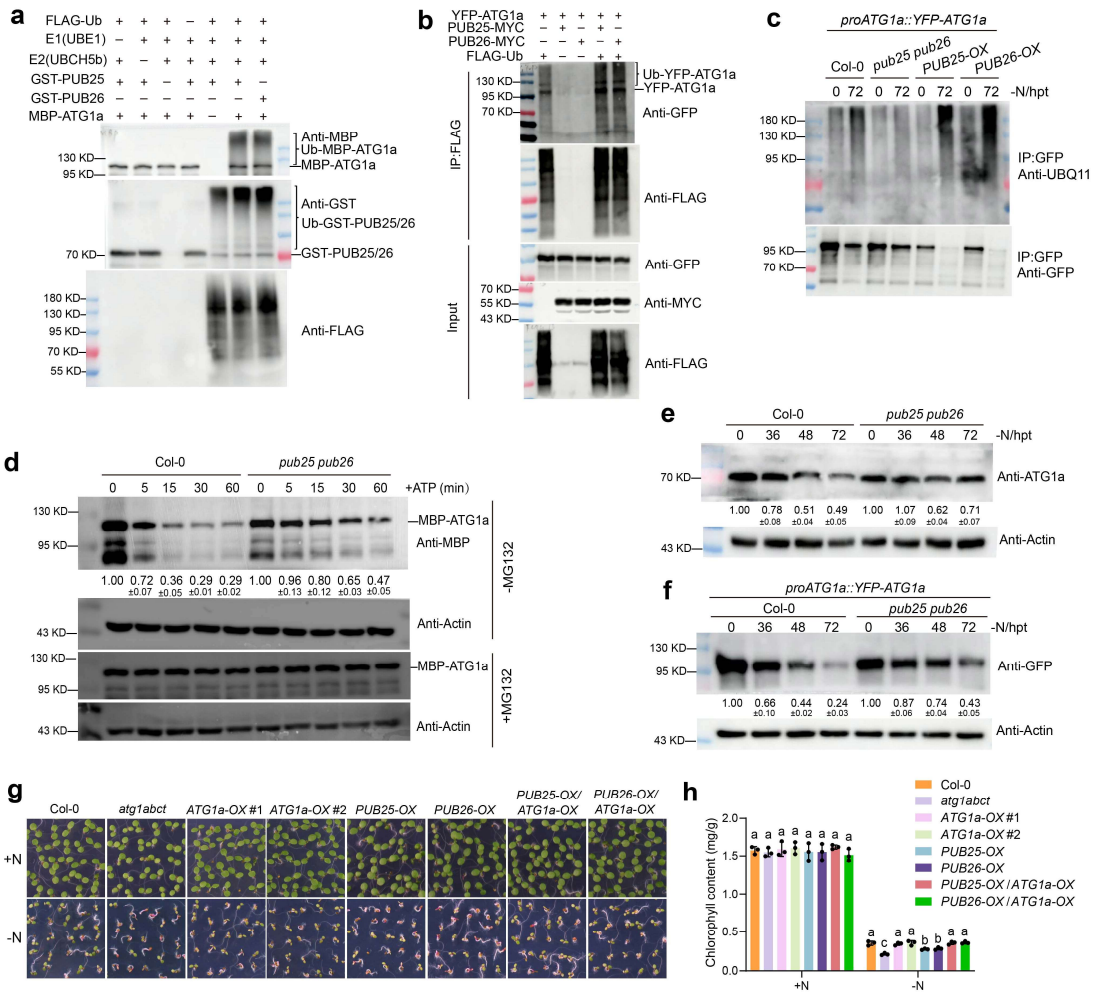

Fig. 3 | PUB25 and PUB26 ubiquitinate ATG1a and promote its proteasomal degradation.

a In vitro ubiquitination of ATG1a by PUB25 and PUB26. Reaction mixtures were incubated with 10 mM ATP at 37°C for 5 h. Ubiquitination was detected with the indicated antibodies. **b** Ubiquitination of ATG1a by PUB25 and PUB26 in protoplasts. Cells co-expressing PUB25-MYC or PUB26-MYC, YFP-ATG1a, and FLAG-Ub were treated with 5 μM MG132 for 16 h. Anti-FLAG immunoprecipitates were immunoblotted with anti-GFP antibody. **c** PUB25 and PUB26-mediated ubiquitination of ATG1a under nitrogen starvation. Transgenic plants stably expressing proATG1a::YFP-ATG1a were subjected to nitrogen starvation, followed by anti-GFP immunoprecipitation and immunoblotting with anti-UBQ11 antibody. **d** PUB25 and

PUB26 promotes ATG1a degradation in cell-free assay. Recombinant MBP-ATG1a was incubated with total protein extracts from Col-0 or *pub25 pub26* in the presence of 1 mM ATP, with or without 5 μM MG132, and detected with anti-MBP antibody. Values below lanes indicate MBP-ATG1a levels normalized to actin. **e** Endogenous ATG1a stability in Col-0 and *pub25 pub26* under nitrogen starvation. Values below lanes indicate ATG1a levels normalized to actin. **f** YFP-ATG1a stability in Col-0 and *pub25 pub26* under nitrogen starvation. Values below lanes indicate YFP-ATG1a levels normalized to actin. For (**d, e, f**), data represent mean ± SD (n = 3). **g** Introduction of 35S::YFP-ATG1a into the *PUB25*- or *PUB26*-overexpression lines restores nitrogen starvation tolerance. **h** Chlorophyll content of seedlings from (**g**). For each biological replicate, at least 64 plants were examined per genotype. Data are mean ± SD (n = 3; one-way ANOVA with Tukey's multiple comparison test, $P < 0.05$).

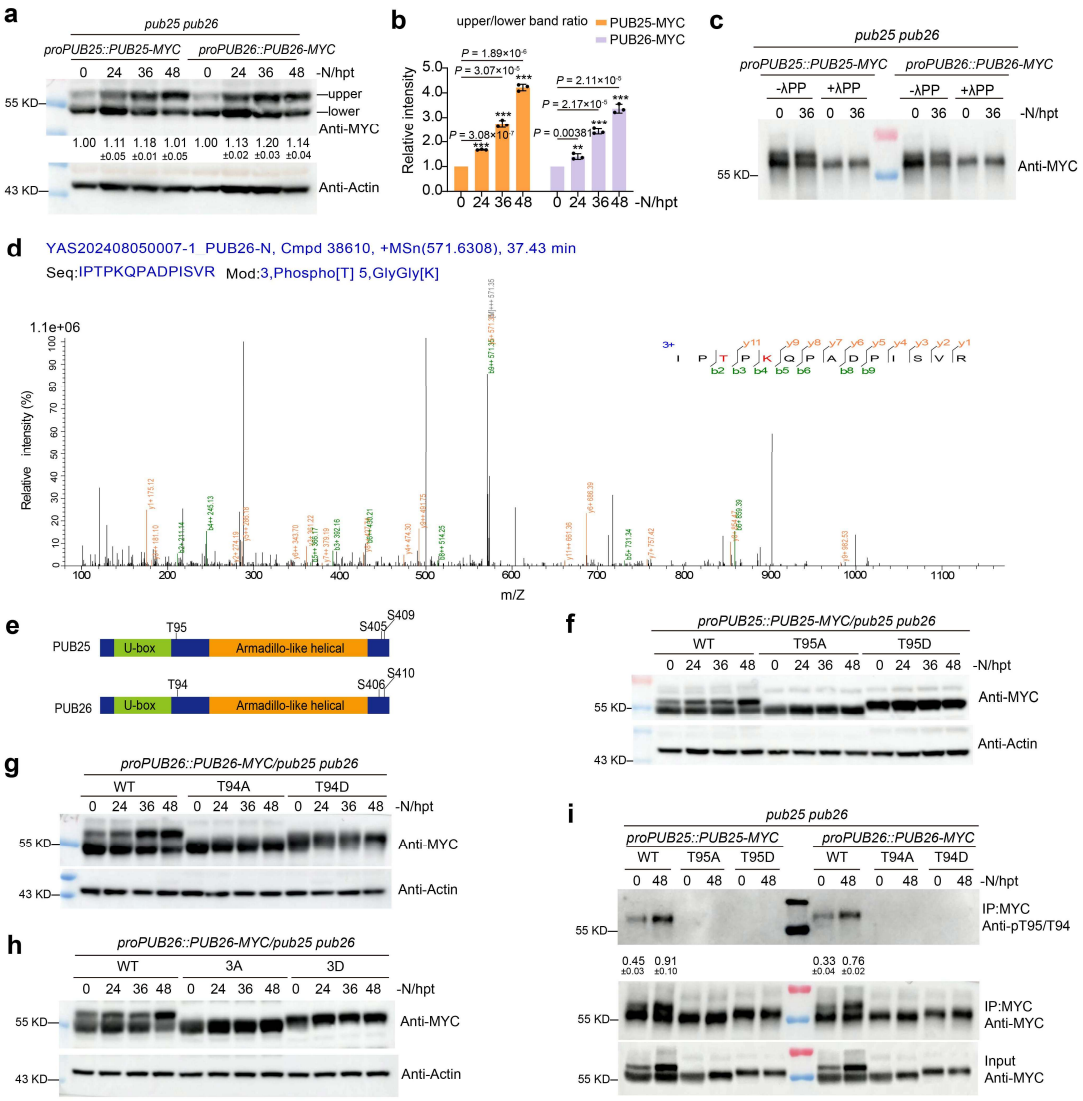

Fig. 4 | Nitrogen starvation induces phosphorylation of PUB25 at Thr95 and PUB26 at Thr94.

a Phosphorylation-dependent mobility shifts of PUB25 and PUB26 under nitrogen starvation. *pub25 pub26* stably expressing proPUB25::PUB25-MYC or proPUB26::PUB26-MYC were subjected to nitrogen starvation for the indicated times and immunoblotted with anti-MYC antibody. Values below lanes indicate total PUB-MYC levels normalized to actin. Data represent mean ± SD (n = 3). **b** Quantification of the ratio of the upper band to the lower band from (**a**). Data are mean ± SD (n = 3, $^{**}P < 0.01$, $^{***}P < 0.001$, two-tailed unpaired Student's t-test). **c** λ-Phosphatase (λPP) treatment confirms that the mobility shift in (**a**) is due to phosphorylation. **d**

Identification of PUB26 Thr94 phosphorylation site by IP-MS. PUB26-MYC was immunoprecipitated from nitrogen-starved *proPUB26::PUB26-MYC/pub25 pub26* seedlings and analyzed by LC-MS/MS. **e** Schematic diagrams showing the identified Thr94 site in PUB26 and the corresponding conserved Thr95 in PUB25. **f, g** Mutations at Thr95 (PUB25) or Thr94 (PUB26) abolish nitrogen starvation-induced phosphorylation. *pub25 pub26* stably expressing wild-type or phosphosite-mutant versions of PUB25-MYC (**f**) or PUB26-MYC (**g**) driven by the native promoters of *PUB25* and *PUB26* were subjected to nitrogen starvation and analyzed by immunoblot. **h** Mutations at Thr94/Ser406/Ser410 abolish nitrogen starvation-induced phosphorylation. Seedlings expressing wild-type or phosphosite-mutant versions of PUB26-MYC in the *pub25 pub26* background were subjected to nitrogen starvation and analyzed by anti-MYC antibody. **i** Phosphorylation of Thr95 (PUB25) or Thr94 (PUB26) confirmed by phospho-specific antibody. Immunoprecipitates using anti-MYC beads were immunoblotted with anti-pT95/T94 antibody. Values indicate phosphorylation signals normalized to PUB-MYC levels. Data represent mean ± SD (n = 3).

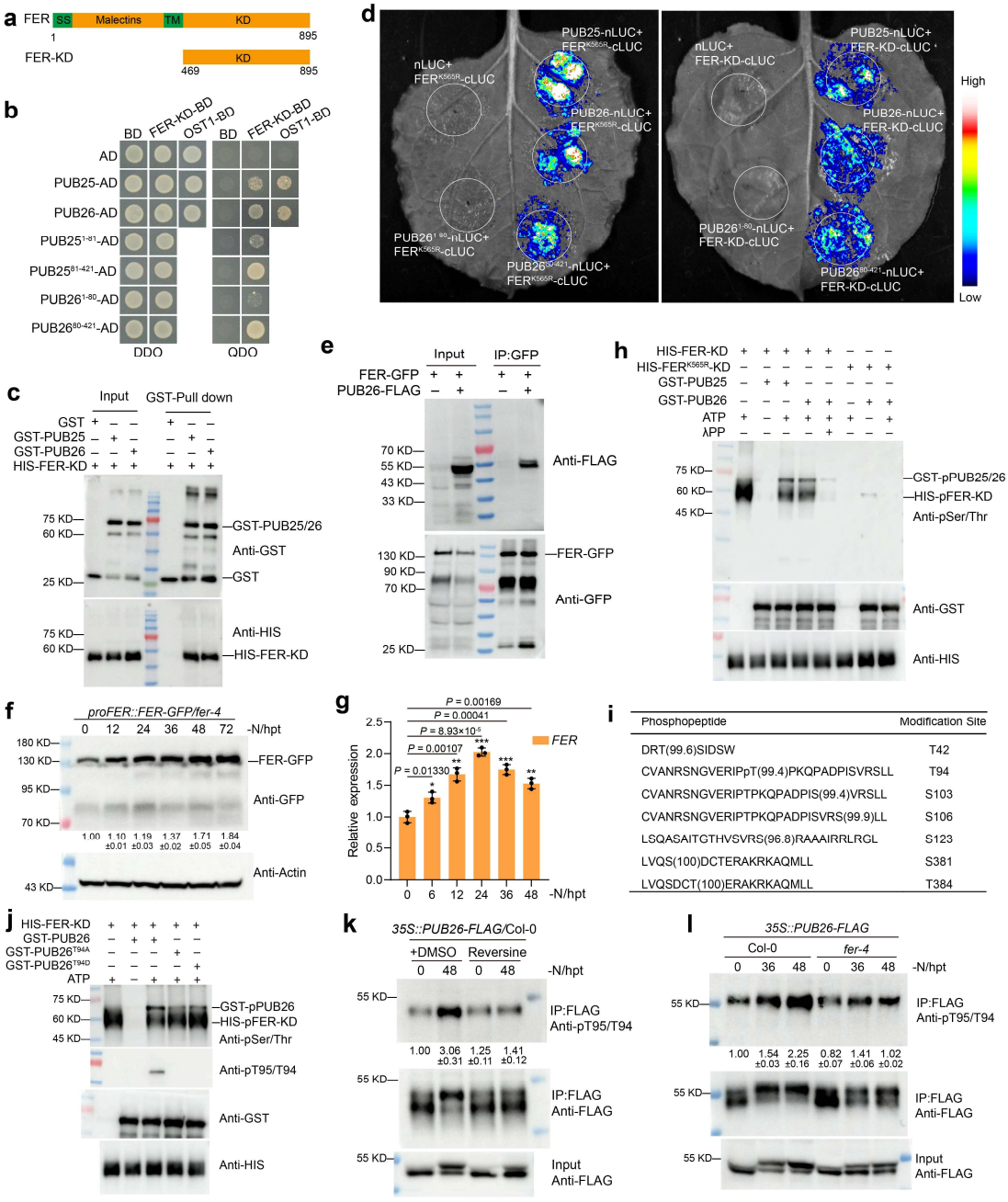

Fig. 5 | The receptor kinase FER directly interacts with and phosphorylates PUB25 and PUB26.

a Schematic of FER domain architecture. SS, signal peptide; TM, transmembrane domain; KD, kinase domain. **b** Y2H assay showing that PUB25 and PUB26 (or their truncated forms) interact with the FER kinase domain (FER-KD). OST1 was used as a positive control. **c** GST pull-down assay detecting interactions between PUB25 and PUB26 and FER-KD. Empty GST was used as a negative control. **d** Split-LUC assays

confirm that PUB25 and PUB26 (or their truncated versions) interact with the full-length kinase-dead variant FER^{K565R} (wild-type FER triggers severe cell death in *N. benthamiana* leaves, so the kinase-dead K565R mutant was used instead) or the truncated FER-KD. **e** Co-IP assay verifying the interaction between FER and PUB26 in Arabidopsis. Total proteins were extracted from transgenic plants co-expressing 35S::PUB26-FLAG and proFER::FER-GFP, immunoprecipitated with anti-GFP beads, and detected by anti-FLAG antibody. **f** Immunoblot analysis of FER stability under nitrogen starvation. Numbers below lanes indicate relative FER-GFP protein levels normalized to actin (mean ± SD, $n = 3$). **g** Transcript levels of *FER* under nitrogen starvation. Data represent mean ± SD ($n = 3$). Asterisks indicate statistically significant differences compared with 0 h (two-tailed unpaired Student's *t*-test: $*P < 0.05$; $**P < 0.01$; $***P < 0.001$). **h** In vitro phosphorylation of PUB25 and PUB26 by FER-KD and FER^{K565R}-KD. Phosphorylated proteins were detected by anti-pSer/Thr antibody, and phosphorylation was confirmed by λ-phosphatase (λPP) treatment. **i** Identification of FER-KD-mediated PUB26 phosphorylation sites by IP-MS. **j** In vitro phosphorylation of PUB26 Thr94 variants by FER-KD. Phosphorylated proteins were detected by anti-pSer/Thr antibody and anti-pT95/T94 antibody. **k, l** Effect of FER inhibitor Reversine (5 μM) (**k**) and FER loss-of-function mutation *fer-4* (**l**) on nitrogen starvation-induced PUB26 Thr94 phosphorylation. Seven-day-old Col-0 and *fer-4* mutant expressing 35S::PUB26-FLAG were subjected to nitrogen starvation. Values indicate phosphorylation signals normalized to the immunoprecipitated PUB26-FLAG levels. Data present mean ± SD ($n = 3$).

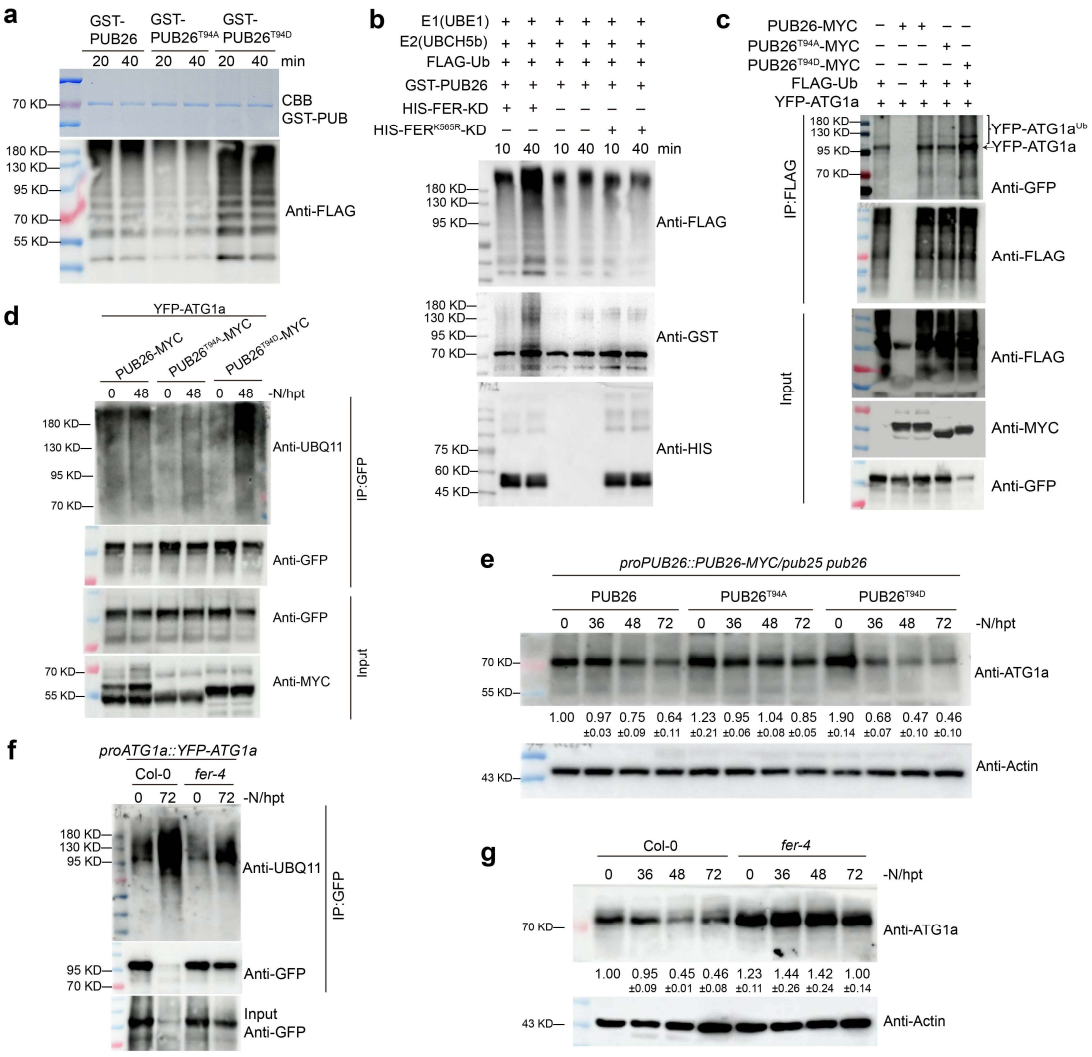

Fig. 6 | FER phosphorylates PUB26 to enhance its E3 ubiquitin ligase activity toward ATG1a.

a Phosphorylation of Thr94 on PUB26 promotes its auto-ubiquitination. In vitro ubiquitination assays were performed with recombinant PUB26 variants (WT, T94A, and T94D) for the indicated durations. Auto-ubiquitination was detected by anti-FLAG antibody. **b** FER-KD-mediated phosphorylation enhances PUB26 E3 ubiquitin ligase activity. Recombinant PUB26 was pre-incubated with FER-KD or FER^{K565R}-KD and ATP to induce phosphorylation, followed by in vitro ubiquitination assays. Reactions were analyzed by anti-FLAG and anti-GST antibodies. **c** PUB26 Thr94 phosphorylation enhances ATG1a ubiquitination in vivo. Protoplasts isolated from the

pub25 pub26 double mutant co-expressing YFP-ATG1a, FLAG-Ub, and PUB26 (WT/T94A/T94D)-MYC were treated with 5 μM MG132. Total proteins were immunoprecipitated with anti-FLAG beads, followed by immunoblotting with anti-GFP antibody. **d** Effect of PUB26 T94 phosphorylation on ATG1a ubiquitination under nitrogen starvation. *pub25 pub26* plants stably expressing YFP-ATG1a and PUB26 (WT, T94A, or T94D)-MYC driven by the PUB26 native promoter were subjected to nitrogen starvation for the indicated times. Total proteins were immunoprecipitated with GFP beads and detected with anti-UBQ11 antibody. **e** Phosphorylation of Thr94 on PUB26 promotes ATG1a degradation under nitrogen starvation. *pub25 pub26* stably expressing PUB26 (WT/T94A/T94D)-MYC driven by PUB26 native promoter were subjected to nitrogen starvation. ATG1a protein levels were detected with anti-ATG1a antibody. Values below lanes indicate ATG1a levels normalized to actin. Data are mean ± SD (n = 3). **f** ATG1a ubiquitination under nitrogen starvation in *fer-4* mutant. Col-0 and *fer-4* mutant expressing proATG1a::YFP-ATG1a were subjected to nitrogen starvation. Proteins were immunoprecipitated with anti-GFP beads and analyzed by anti-UBQ11 antibody. **g** ATG1a degradation in Col-0 and *fer-4* under nitrogen starvation. Total proteins were extracted and immunoblotted with anti-ATG1a antibody. Values below lanes indicate ATG1a levels normalized to actin. Data are mean ± SD (n = 3).

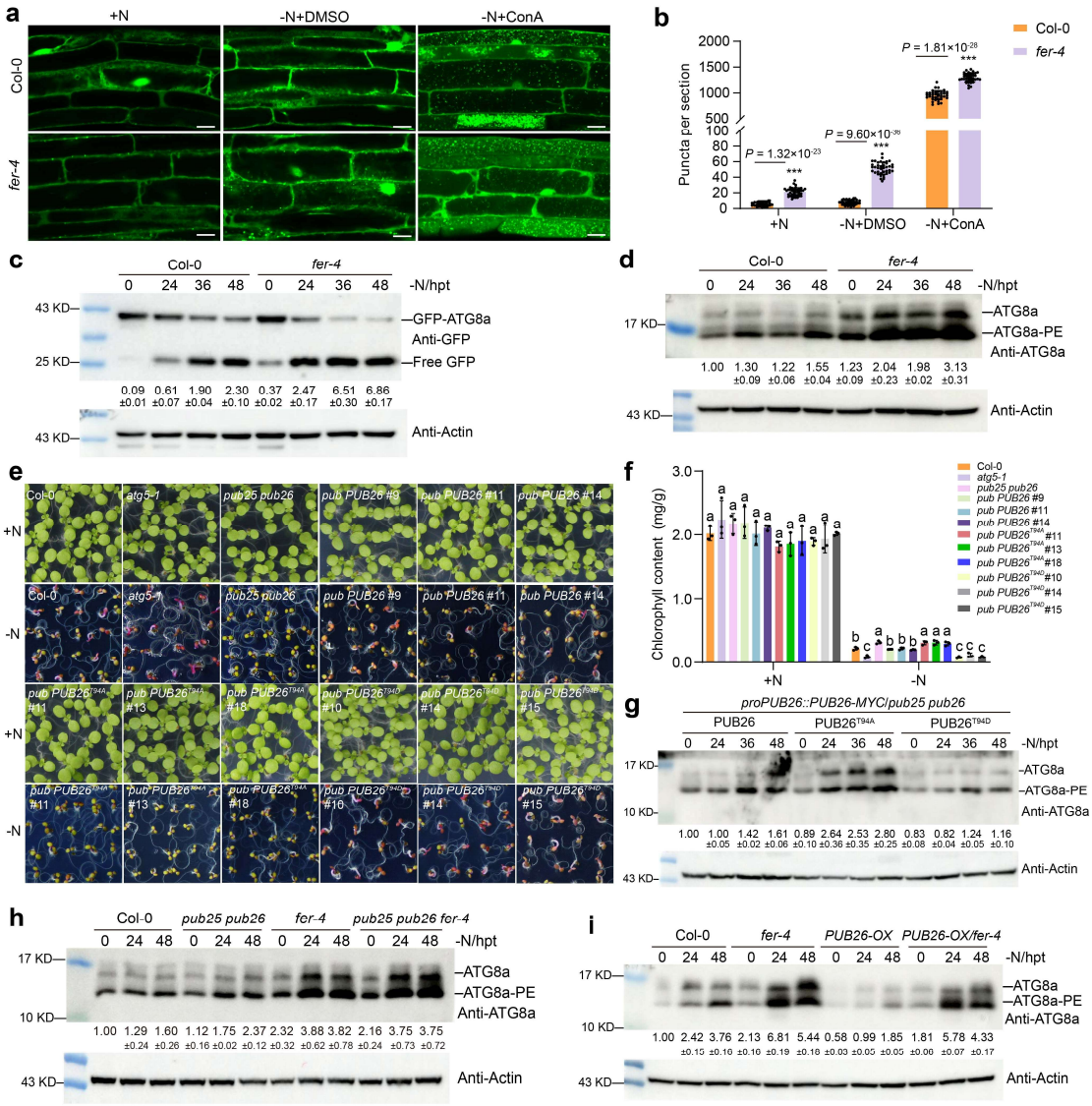

Fig. 7 | FER-mediated phosphorylation of PUB26 negatively regulates nitrogen starvation-induced plant autophagy.

a Accumulation of GFP-ATG8a-labeled autophagic bodies in the central vacuole of Col-0 and *fer-4* mutant. Scale bar = 20 μm. **b** Quantification of autophagosome puncta from (**a**). Four images per seedling were quantified (10 seedlings per treatment). Data represent means ± SD (n = 40; ***P < 0.001, two-tailed unpaired Student's t-test). **c** GFP-ATG8a processing in Col-0 and *fer-4* under nitrogen starvation. Immunoblots were probed with anti-GFP antibody. Free GFP/GFP-ATG8a ratios are shown below lanes. Data are mean ± SD (n = 3). **d** ATG8a lipidation in Col-0 and *fer-4* under nitrogen

starvation. **e** PUB26 Thr94 phosphorylation enhances plant sensitivity to nitrogen starvation. *pub25 pub26* plants expressing PUB26 Thr94 variants (wild-type, T94A, and T94D) driven by the PUB26 native promoter were grown on 1/2 MS medium with or without nitrogen for 6 days. **f** Chlorophyll contents of seedlings in (**e**). Data are mean ± SD (n = 3 independent biological replicates, with at least 64 plants examined per replicate). Different letters indicate statistically significant differences (one-way ANOVA followed by Tukey's multiple comparison test, $P < 0.05$). **g** PUB26 Thr94 phosphorylation suppresses nitrogen starvation-induced autophagy. Protein extracts from nitrogen-starved *pub25 pub26* expressing PUB26 Thr94 variants (as in **e**) were immunoblotted with anti-ATG8a antibody for the indicated times. **h** ATG8a lipidation in Col-0, *pub25 pub26*, *fer-4* and *pub25 pub26 fer-4* plants under nitrogen starvation. **i** ATG8a lipidation in Col-0, *fer-4*, *PUB26-OX*, and *PUB26-OX/fer-4* plants under nitrogen starvation. For (**d, g, h, i**), ATG8a-PE levels normalized to actin are shown below lanes. Data are mean ± SD (n = 3). hpt, hours post-treatment.

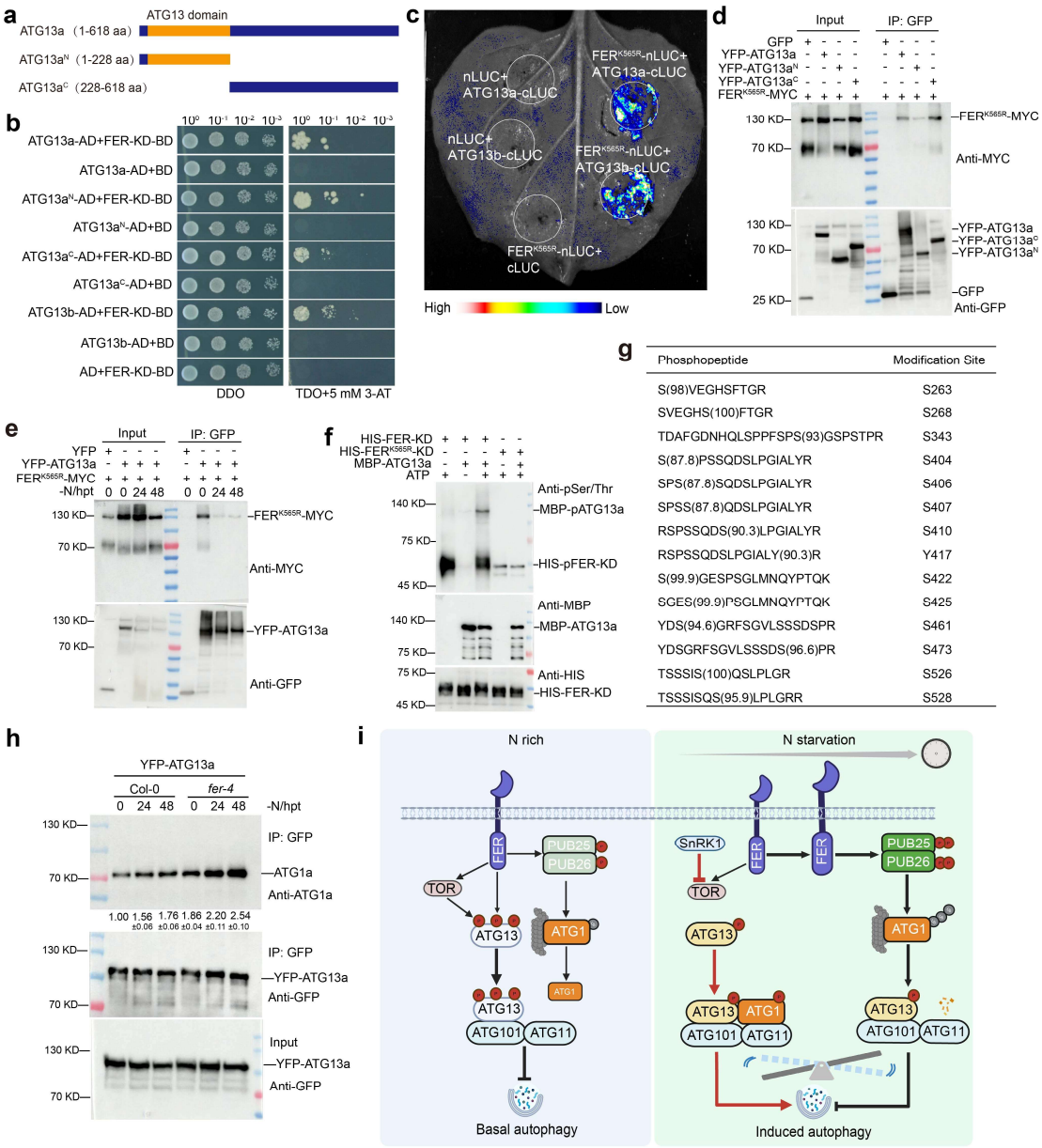

Fig. 8 | FER directly interacts with and phosphorylates ATG13 to inhibit ATG1-ATG13 complex formation.

a Schematic representation of the predicted domains in ATG13a, as well as truncated N- and C-terminal regions. **b** Y2H assays showing interactions between FER-KD and ATG13a or ATG13b. **c** Split-LUC assays confirming interactions between FER^{K565R} and ATG13a or ATG13b in *N. benthamiana* leaves. **d** Co-IP assays validating the interaction between FER^{K565R} and ATG13a. Total proteins were extracted from *N. benthamiana* leaves co-expressing FER^{K565R}-MYC with YFP-ATG13a, YFP-$ATG13a^{N}$,

or YFP-ATG13a^{C}, followed by immunoprecipitation with GFP beads and immunoblotting with anti-MYC antibody. **e** Interaction between FER^{K565R}-MYC and YFP-ATG13a under nitrogen starvation conditions. Total proteins were extracted from Arabidopsis 35S::YFP-ATG13a overexpression plants at the indicated time points after nitrogen starvation, followed by immunoprecipitation using GFP beads. The purified beads were then incubated with FER^{K565R}-MYC protein transiently expressed in *N. benthamiana* leaves, and detected using anti-MYC antibody. **f** In vitro phosphorylation assays of ATG13a by FER-KD and FER^{K565R}-KD. Recombinant proteins were incubated in phosphorylation reaction buffer containing 1 mM ATP at 30°C for 30 min. Phosphorylated proteins were detected by anti-pSer/Thr antibody. **g** Identification of FER-KD-mediated ATG13a phosphorylation sites by IP-MS. The phosphorylated ATG13a bands from the in vitro phosphorylation reaction in (**f**) were excised and analyzed by mass spectrometry. **h** The interaction of ATG1a and ATG13a in Col-0 and *fer-4* upon nitrogen starvation. Col-0 and *fer-4* expressing 35S::YFP-ATG13a were subjected to nitrogen starvation for the indicated times. Total proteins were extracted, immunoprecipitated with GFP beads, and detected with anti-ATG1a antibody. Values below each lane represent the ratio of ATG1a to ATG13a. Data are mean ± SD (n = 3). **i** A proposed working model for FER-mediated regulation of PUB25 and PUB26 in autophagy control in Arabidopsis.

Supplementary Files

This is a list of supplementary files associated with this preprint. Click to download.

- DescriptionofAdditionalSupplementaryFiles4.28.docx
- SupplementaryData3.4.28.xlsx
- SupplementaryData4.4.28.xlsx
- SourceDataforMainFigures4.28.xlsx
- reportingsummary4.28.pdf
- SupplementaryData2.4.28.xlsx
- SourceDataforSupplementaryFigures4.28.xlsx
- SupplementaryFigure4.28.pdf
- SourceDataforUncroppedWBgels4.28.xlsx
- SupplementaryData1.4.28.xlsx